Journal of Fluids and Structures (1999) **13,** 519–548
Article No.: jfls.1999.0218 available online at http://www.idealibrary.com on IDEAL

FLUID–STRUCTURE RESONANCE PRODUCED BY ONCOMING ALTERNATING VORTICES

R. M. C. So

Mechanical Engineering, The Hong Kong Polytechnic University
Hung Hom, Kowloon, Hong Kong

I. Jadic and M. P. Mignolet

Mechanical and Aerospace Engineering, Arizona State University
Tempe, AZ 85287-6106, U.S.A.

(Received 15 May 1998 and in revised form 26 February 1999)

The present investigation examines a simple fluid–structure interaction problem, which is represented by the unsteady response of an airfoil/blade to a Karman vortex street in an inviscid uniform flow. Two different cases were examined; one with a rigid airfoil/blade, where the structural stiffness is infinite, another with an elastic blade. In both cases, the flow remains attached to the airfoil/blade surface. A time-marching technique solving the Euler equations and a two-degree-of-freedom structural dynamic model is used to examine the interactions between the fluid and the structure. The interactions between the convected vortices and the structure modify the shed wake whose energy, in turn, feeds into the forces and moments acting on the structure. For a rigid airfoil/blade, it is found that the amplitude of the aerodynamic response is not proportional to the density of the oncoming vortex street, but depends on c/d, the ratio of the chord length (c) to the axial spacing (d) of the convected vortices. When the number of vortices per unit length is increased, the amplitudes of the aerodynamic response increase and then decrease even though the density of the vorticity keeps increasing and so is the energy of the excitation wake. Maxima are observed at $c/d = 0{\cdot}5$, $1{\cdot}5$ and $2{\cdot}5$. This behaviour is analogous to the structural resonance phenomenon and is labeled "aerodynamic resonance". The existence of such an "aerodynamic resonance" is important to turbomachinery applications where the blade is elastic, the flow is unsteady and the shed vortices from the previous row are convected downstream by the mean flow. Thus, "aerodynamic resonance" alone or in conjunction with structural resonance could impact negatively on the fatigue life of turbine blades and their combined effects should be accounted for in blade design. A preliminary attempt to assess this impact has been carried out. It is found that the relative fatigue life of a blade could be reduced by four orders of magnitude as a result.

1. INTRODUCTION

Flow-induced vibrations are of common occurrence in different engineering disciplines; these include forced and free vibration problems. The use of the terms "forced" and "free" needs clarification. In this paper, the term "forced vibration" is used to denote the class of problems where the excitation forces consist of both externally imposed (mechanical and flow-related) and flow-induced forces. Thus, they include such external forces as those generated by turbulence, gust and vortices in the free-stream. For example, the investigations of Gopalkrishnan *et al.* (1994) and Streitlien *et al.* (1996) are an example of one type of

0889–9746/99/040519 + 31 $30.00

forced vibration problems. They considered the motion of an oscillating airfoil in a uniform stream with a row of vortices superimposed on it. The airfoil oscillations are externally imposed. In both studies, the oscillations of the airfoil generated by flow-induced forces, whether they are created by the oncoming vortices or by the induced motion of the shed wake, are not considered. As a result, the important parameter is the phase between the mechanically induced airfoil motion and the arrival of the free-stream vortices. The "forced vibration" problem is different from the "free vibration" case where there is no external excitation, be it mechanical or due to disturbances in the oncoming flow, and the motion of the structure is a consequence of the flow-induced forces created by the shed wake alone. A typical example of free vibration is the flutter problem (Fung 1993; Hall 1994).

The present paper considers a "forced vibration" problem that is slightly different from that treated by Gopalkrishnan *et al.* (1994) and Streitlien *et al.* (1996). In the present problem, the external excitations are created by oncoming vortices only and the airfoil/blade is considered to be either rigid or elastic. Here, a rigid structure implies one with infinite structural stiffness. Two separate cases are considered; one is represented by a rigid airfoil/blade, another deals with an elastic airfoil/blade. Note that, in the elastic case, the structure will also respond to the flow-induced forces created by the shed vortices. The presence of this feedback indicates that the case investigated is a tightly coupled fluid–structure interaction problem as opposed to the structurally driven situation considered by Gopalkrishnan *et al.* (1994) and Streitlien *et al.* (1996). There are different kinds of flow-induced vibration phenomena associated with this simple forced vibration problem. Prominent among them are the buffeting and the Strouhal excitation, which are discussed here to highlight the fluid–structure interactions of the present forced vibration problem.

Before discussing Strouhal and buffeting excitations, the difference between vibrations created by the flow-induced motion of the structure and by the oncoming vortical flow needs to be clarified. The one-degree-of-freedom dynamic equation is used as an example to illustrate. This equation can be written as (Lalanne *et al.* 1983)

$$m\ddot{x} + kx = F_1(t) + F_2(t), \tag{1}$$

where m is the mass of the structure, x is its displacement and k is its structural stiffness. Here the dot is used to denote differentiation with respect to time. Note the absence of a structural damping term of the form, $C_{st}\dot{x}$, in the above model.This assumption is justified because the damping ratio of most metallic structures, $\eta = C_{st}/2\sqrt{km}$, is extremely low, thus the fluid damping effects dominate. The unsteady forces, generated by the fluid flow, have been decomposed into two components, $F_1(t)$ and $F_2(t)$. According to Naudascher and Rockwell (1994), $F_1(t)$, which is generated exclusively by the motion of the blade, is denoted as a movement induced excitation (MIE). The flutter phenomenon, for which $F_2(t) = 0$, has been categorized as an MIE problem because the remaining force $F_1(t)$ on the right-hand side of equation (1) depends entirely on the structural response of the system and its time history (Jadic *et al.* 1998). In fact, the only reason why $F_1(t)$ is on the right-hand side of equation (1) is its fluid flow origin. For the freestream vortex-induced vibration problem considered here, the response is driven by forces that are created by the oncoming vortices and are external with respect to the fluid–structure system, i.e. $F_2(t) \neq 0$. Following Naudascher & Rockwell (1994), this external system of forces is denoted as an extraneously induced excitation (EIE). Clearly, however, MIE is also present, i.e. $F_1(t) \neq 0$ as well.

Traditionally, the word buffeting is used to describe the response of a rigid structure to a turbulent wind, while Strouhal excitation refers to the rigid structure response to a laminar flow, where the shed wake is not modified by the upstream flow. The turbulent flow could be stationary or nonstationary. In addition, discrete vortices could be present in

a laminar or a turbulent freestream. Under these conditions, the nature of the flow-induced forces could be modified significantly compared to a Strouhal or buffeting excitation in the absence of discrete vortices. The unsteady buffeting forces would become broad base with multiple frequency components (So & Savkar 1981; Baban & So 1991) which come about as a result of the interactions between the wake and the oncoming turbulent flow. If the structure is also elastic, both the buffeting and the Strouhal phenomena become more complicated. In this latter case, the motion of the structure and its effect on the unsteady wake could further modulate the flow-induced forces. This problem has received scant attention to date. However, the problem is of growing concern to engineers working in the area of fluid–structure interactions, especially in the turbomachinery and nuclear fields.

Each blade row in a multistage turbomachine generates wakes that are convected into the downstream blade row. The flow in the blade passage is usually turbulent because of the very high Reynolds number. Consequently, if the coordinates are fixed with respect to the downstream blade row, the oncoming turbulent mean flow with the convected vortices generated by the upstream blades would appear to be unsteady. Thus, the fluid–structure interactions associated with the blades are very complicated (Feiereisen *et al.* 1994). The lack of understanding of this problem leads to tremendous uncertainty in the estimates of blade life and their fatigue failure. Numerous techniques have been proposed to treat this problem. A summary of these techniques has been given by Majjigi & Gliebe (1984). Quite often, these techniques assumed that the induced forces are not coupled with the structural deformations. As such, the unsteady flow-induced forces can be considered as external excitation to the structures. Also, decomposition of the vortices into Fourier components are usually assumed. In other words, the effects of the upstream vortices are described in terms of their harmonics, with each harmonic modeled as a forcing function boundary condition for the prediction of the corresponding harmonic of the unsteady aerodynamic response (Feiereisen *et al.* 1994). Such a treatment of the problem is rather incomplete and leaves the real interactions between the fluid, the vortices, the wake and the structure unresolved.

Other methods of analyzing the fluid–structure coupling problem have been proposed by researchers to treat structures besides airfoils/blades. They include finite element and finite difference approaches. Finite element simulations of both the structural and fluid domains allow the treatment of very complex geometric boundary conditions at the expense of a greatly simplifying flow field. As a result, the upstream flow is considered to be inviscid, irrotational and uniform [e.g., Zienkiewicz & Bettes (1978), Olson & Bathe (1985), Xing & Price (1991)]. An improved approach, still uses finite elements, solves the Navier–Stokes equations rather than the pressure or velocity potential equation alone (Casadei & Halleux 1995). The advantage of this approach is its ability to deal with complex geometry without having to make unnecessary assumptions about the flow field. In finite difference treatments, the structural dynamic system is usually modeled by an N-degree-of-freedom system. A time-marching technique is used to solve the unsteady governing equations consisting of both the Navier–Stokes and the modeled structural dynamics equations. This approach treats the flow equations implicitly and the structural dynamic equations explicitly, so that the coupled integration time steps of the fluid and structure can be matched more appropriately (Bélanger *et al.* 1995). However, in these approaches, the upstream flow is usually assumed to be irrotational. Hence, the effect of the upstream vortices on the strctural response has not been treated. If the flow-induced vibration problem in a turbomachine environment is to be understood, it is necessary to first examine the the effects of upstream vortices on the fluid–structure interaction problem.

Recently, as part of this research, a time-marching technique has been developed by Jadic *et al.* (1998) to treat flow-induced vibration problems in turbine blades where the oncoming

flow is vortical and there is no separation on the blades. The approach makes use of a boundary element method to determine the flow field, an operator-splitting technique (Chorin 1973) to solve for the convection and diffusion of vorticity, including upstream and wake vorticity, a free wake model to simulate the trailing vortices shed from the turbine blade (Yao *et al.* 1989) and a two-degree-of-freedom model for the structural dynamics behaviour. Jadic *et al.* (1998) used the technique to re-examine the airfoil flutter problem (Hall 1994), the existence of limit-cycle oscillations (LCO) and the source of nonlinearity in the flutter problem, and the effects of structural nonlinearity on the LCO of the airfoil. The nonlinear characteristics and the LCO are not evident from the linear solution of Hall (1994). They result from the proper treatment of the fluid–structure interactions, which include the wake interactions with the airfoil, and the interactions of the upstream vortices with the airfoil and the wake if there are oncoming vortices in the freestream. This technique, therefore, allows a rather general upstream flow, with or without vortices and their interactions with the structure, to be treated in a formal way and represents an improvement over that proposed by Bélanger *et al.* (1995). With the availability of this tool, the fluid–structure interaction problem related to turbomachines could be examined in more detail.

The blades in a blade row are subject to vibrations as a result of upstream generated disturbances propagated by the freestream velocity. Thus, the external excitations are represented by flow disturbances and the problem of interest here is to find out the underlying principles that govern the fluid–structure interactions, in particular the resonant behaviour of the fluid–structure system. For a purely structural problem with $F_2(t)$ being a harmonic force, resonance occurs when the frequency of the external excitation is equal to the natural frequency of the structural system. In the case of such "mechanical" resonance, the amplitude of oscillations will increase without bounds while, at the same time, the work produced by the external force would go to infinity when there is no structural damping. For the flow-induced vibration problem studied here, unlike the purely structural resonance problem mentioned above, the amplitudes of the resonant oscillations, even in the absence of structural and viscous damping, would not increase indefinitely because the fluid flow damping would extract energy from the structure thus leading to large but finite amplitudes of response. The high cycle fatigue (HCF) problem in turbomachines is associated with the damage accumulated by the correspondingly large but finite stresses. Therefore, it is of fundamental importance and should be treated first.

The present paper concentrates on flow-induced vibrations created by the oncoming vortical flow. In the case of turbomachines, this vortical flow is given by the oncoming vortices generated by the upstream blade row. These vortices are shed from the upstream blades in an alternating manner, hence, their interactions with the downstream blades will give rise to a quite different phenomenon compared to a single vortex row treated by Jadic (1997). If the effects of the upstream vortices on the downstream blades are to be investigated first, the turbomachine blade vibration problem can be idealized by an upstream flow with a finite number of frequency components, such as that represented by two or more rows of alternating vortices. As a first attempt, the wide range of frequencies found in a turbulent flow is neglected. The structure is assumed to be an airfoil or a turbine blade, so that the technique developed in the first paper (Jadic *et al.* 1998) is directly applicable. As such, the treatment is only valid for flows without separation.

2. THEORETICAL AND NUMERICAL FORMULATIONS

2.1. Numerical Formulation

The starting point of this analysis is the Euler equation. The flow is assumed to be incompressible, two-dimensional and unsteady and the equations are made dimensionless

by the reference velocity, U_∞, and the chord length, c. The equation for the vorticity $\boldsymbol{\omega} = \nabla \times \mathbf{V}$, where $\mathbf{V}$ is the local velocity vector, can be deduced by taking the curl of the Euler equation. In the present study, the main interest is in the influence of an upstream source of vorticity, which is approximated by one or more concentrated "traveling" vortices, on a downstream structure. Therefore, it is justified to neglect viscous diffusion as the first approximation and considered the flow to be inviscid. The circulation Γ around a given material curve is supposed to remain unchanged during the time step δt. Consistent with this approach, it is also assumed that, during this δt the flow behaves like an inviscid "conveyor" of the vorticity which is "frozen". In mathematical terms, this can be written as

$$\mathbf{x}_i^v(t + \delta t) = \mathbf{x}_i^v(t) + \mathbf{V}_0(\mathbf{x}_i^v(t), \omega_i(t)\, t)\, \delta t, \quad i = 1, 2, \ldots, N, \tag{2}$$

where $\omega_i(t)$ is the strength of the ith vortical element, $\mathbf{x}_i^v(t)$ is the position vector of the ith vortical element and N is the number of vortical elements. The suffix "o" in $\mathbf{V}$ is used to denote the convective velocity generated by an inviscid flow. The set of equations (2) is in fact an explicit finite difference form of the differential set of equations which relate (track) the position of a certain vortical element to the velocity of the inviscid flow at that particular location.

The flow around the structure, which is simulated by a distribution of sources and discrete vortices, is solved using a boundary element method for inviscid incompressible flows. The boundary condition applied on the structure surface (flow tangency condition) is $(\mathbf{V}_0 - \mathbf{V}_s)\cdot \mathbf{n} = 0$, where $\mathbf{V}_s$ is the velocity of the structure surface. The far-field boundary condition is given by $\mathbf{V}_0 = \mathbf{V}_\infty + \mathbf{V}_\omega$, where $\mathbf{V}_\infty = \mathbf{i}U_\infty$, $\mathbf{V}_\omega$ is the rotational part of $\mathbf{V}_0$, and $\mathbf{i}$ is the unit vector along the stream direction, x. Solving the given boundary equations yields the source and vorticity distributions on the structure surface. Then, succesively, the flowfield velocities and pressure distributions are calculated. Further details concerning this formulation can be found in Jadic (1997), Jadic *et al.* (1998) and an earlier paper by Yao *et al.* (1995). The interested reader is referred to these references. Once the velocity and pressure fields are known, the unsteady forces and moment on the structure can be determined by integrating around the airfoil/blade.

It should be pointed out that the flow over the airfoil has to remain attached in order that the free wake model (Yao *et al.* 1989) assumed is still valid. In addition, the methodology used to track the oncoming vortices has been developed by Yao (1993) and is adopted in the present calculations. Further, the fluid–structure interactions are fully resolved by iterating between the fluid governing equations and the structural dynamics equations at each time step until a convergent solution is obtained. Since the present objectives are to investigate the aerodynamic and structural resonance arising from interactions between the oncoming vortices, the structure and the wake, as a first attempt, the effects of viscosity could be neglected and the freestream could be assumed to be uniform in the absence of oncoming vortices. Therefore, U_∞ is taken to be constant in the transverse direction, y.

The dynamic response of the structure is in general governed by a set of partial differential equations if the mass is continuously distributed, and/or ordinary differential equations if the structure is approximated by lumped masses. Although these equations are often assumed to be linear, nonlinear terms can appear due to geometric factors (large rotations, intermittent contact of shrouds, etc.) or to the material properties of the structure (large deformations, inelastic behavior). In the context of airfoils and turbomachine blades, the simple two-degree-of-freedom structural model can be assumed. The equations of motion are

$$m\ddot{h} - (ma\cos\theta)\,\ddot{\theta} + k_h h + (ma\sin\theta)\,\dot{\theta}^2 = L. \tag{3a}$$

$$I\,\ddot{\theta} - (m\,a\cos\theta)\,\ddot{h} + k_\theta \theta = M, \tag{3b}$$

where h is the plunging displacement of the blade, which models the bending deformations, and θ is the pitching angle of the blade, which is representative of torsional deformations. The coefficient a is the distance between the elastic axis and the center of mass, m is the mass of the blade section per unit spanwise length, I is the moment of inertia of the blade section, k_h and k_θ are the bending and torsional stiffnesses, $L = (\frac{1}{2})\, C_L \rho\, U_\infty^2 c$ and $M = (\frac{1}{2}) C_M \rho\, U_\infty^2 c^2$ are the aerodynamic lift and moment acting on the blade, C_L and C_M are the lift and moment coefficients and ρ is fluid density. These equations are solved iteratively together with the fluid equations in order to resolve the fluid–structure interactions properly.

2.2. Data Analysis

The present calculations yield time series for the forces, the displacements and the velocity field. These time series are analyzed using the auto-regressive moving averaging (ARMA) identification technique (Mignolet and Red Horse 1994). This approach relies on the evaluation of the likelihood function corresponding to measured or calculated (if in a numerical simulation experiment) time-series data. There are several steps in this multi-stage approach. First, it represents the time series data using an AR (auto-regressive) model, which predicts the present values as a linear combination of the past values and a white noise deviate. The model is obtained by solving a linear system of equations. These results are then used to initialize an MA (moving-averaging) matrix polynomial. Afterwards, an iterative procedure is employed to determine the ARMA model that provides, at the same time, a "best" fit of both the time series data and the AR model. Finally, the estimates of the natural frequencies, damping ratios and mode shapes are obtained from the auto-regressive part of the ARMA model. A more detailed discussion of this technique can be found in Mignolet *et al.* (1993), Mignolet & Red Horse (1994) and Jadic *et al.* (1998).

Finally, it should be pointed out in this paper that a *negative* damping will be indicative of a "dissipation" on the structure, including an energy transfer to the fluid.

2.3. External Excitation Model

In order to analyze the problem discussed in the foregoing, it is necessary to first define the type of external excitations to be considered. Throughout this investigation, the forcing function will consist of a series of flow-convected vorticity perturbations considered to be released in the flow, e.g. by an upstream blade row. The possibility of using concentrated vortices to represent these vorticity perturbations has been investigated by many researchers, including Christiansen (1973), Chorin (1973), and Clements & Maull (1975). Further, Poling *et al.* (1989) have used a discrete vortex model similar to a Karman vortex street (KVS) to describe the excitation encountered by a helicopter blade. Funazaki and Nishiyama (1989) and Feiereisen *et al.* (1994) have carried out a series of experiments on interaction phenomena in turbomachinery, in which the upstream blade row was represented by a set of circular bars moving ahead of a stator row. Also, Gopalkrishnan *et al.* (1994) used an upstream cylinder to generate the vortex street, while Streitlien *et al.* (1996) specified a KVS in their treatment of an oscillating airfoil in a vortical flow. The experimental setups led to excitation patterns similar or identical to the KVS. Finally, Hodson & Dawes (1996) presented further evidence that the rotational flow through a blade row exhibits features similar to those of a periodic and discrete vortex street.

In view of these findings, the present investigation adopts the KVS pattern as the external excitation model. The computational configuration is as shown in Figure 1. The free-stream velocity is U_∞, the chord length of the blade is c and the spacing of the vortices is d. Based

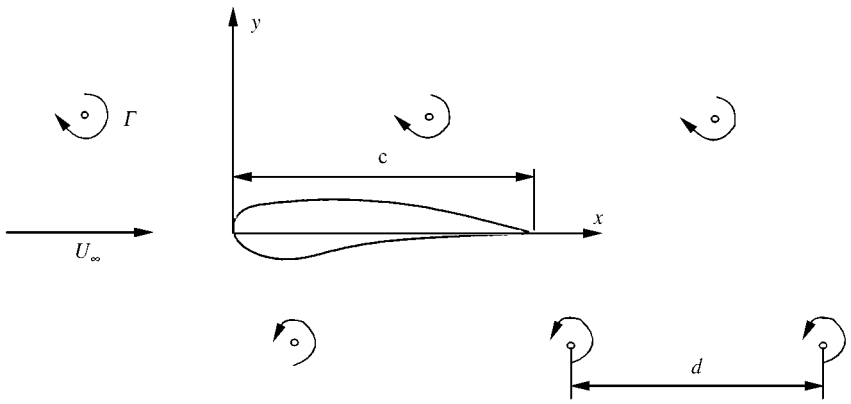

Figure 1. An idealized fluid–structure interaction problem.

TABLE 1

Harmonic composition of the KVS pattern

Harmonic	Amplitude of u	Amplitude of v
1	0	1
2	0·58732	0
3	0	0·34577
4	0·20312	0

on these quantities, a frequency parameter, U_∞/d, can be defined, which after normalization of the equations by U_∞ and c reduces to c/d. The fundamental frequency of the EIE mode is, therefore, given by c/d.

Unlike the single harmonic perturbation pattern used by Knoller (1909), Betz (1912) and Katzmayr (1922), the KVS pattern has a limited number of higher harmonic/Fourier components. Furthermore, the vertical velocity plays an important role in the energy transfer. The relative importance of the different harmonics of the streamwise (u) and vertical (v) perturbation velocities on the axis of the KVS is compared in Table 1. Note that the amplitudes of these Fourier coefficients have been obtained through a numerical integration of u and v and are further normalized by the amplitude of the first harmonic of v. It can be seen that the amplitude of the third harmonic of v is 35% of that of the first harmonic. This could have a significant effect on the induced structural response.

2.4. FATIGUE LIFE ESTIMATE

The failure of a mechanical system can be defined in a variety of ways. In the context of turbomachinery blades, however, there are two fundamental mechanisms, i.e. flutter and fatigue. The potential for flutter is easily assessed by using the natural frequencies and damping ratio estimates obtained from ARMA (Jadic *et al.* 1998). Indeed, flutter will not occur if all the damping ratios estimated by this technique are negative. On the contrary, flutter will occur if any of these values is positive. The mode in which flutter will manifest itself is the mode shape corresponding to the most positive damping ratio.

The determination of the fatigue life of the structure can also be achieved from the m natural frequencies (ω_i) and the damping ratios (ζ_i) obtained from ARMA modeling of the stresses $\sigma(t)$ in the blade. Once these characteristics are available, the magnitudes of the different frequency components of $\sigma(t)$ can be obtained by first minimizing the least-squares modeling error,

$$\sum_{k=1}^{n}\left[\sigma(k\,\Delta t)-\sum_{i=1}^{m}\exp(-\xi_i\omega_i k\Delta t\,(\sigma_i^{(c)}\cos(\omega_{di}k\,\Delta t)+\sigma_i^{(s)}\sin(\omega_{di}k\,\Delta t)))\right]^2, \tag{4}$$

where $\omega_{di}=\omega_i\sqrt{1-\xi_i^2}$ with respect to the unknown components, $\sigma_i^{(c)}$ and $\sigma_i^{(s)}$, of the transient structural response. Having solved the corresponding linear system of equations, the magnitude σ_i of the ith frequency component of the stress $\sigma(t)$ is given by

$$\sigma_i=\sqrt{[\sigma_i^{(c)}]^2+[\sigma_i^{(s)}]^2}\,. \tag{5}$$

The number of cycles that the structure will last can be estimated from the S–N curve, which gives the number of cycles (N_i) that will be required for failure under an alternative stress of magnitude σ_i. A classical approximation of the failure estimate is

$$N_i=(\bar{\sigma}/\sigma_i)^{1/K}, \tag{6}$$

where $\bar{\sigma}$ and K are material constants which will be assumed known here. The fatigue life of the structure under the combined effects of all the stress components σ_i, $i=1,2,\ldots,m$, can then be estimated by using Miner's rule (Dieter 1986) which states that at failure

$$\sum_{i=1}^{m}D_i=1, \tag{7}$$

where the individual damage D_i is given by the ratio of the actual number of cycles performed (corresponding to the ith frequency and amplitude of the stress) to the number of cycles that would lead to failure if that component was acting alone. Combining equations (6) and (7), an estimate of the fatigue life is obtained as

$$T=2\pi\Big/\sum_{i=1}^{m}\omega_i/N_i\,. \tag{8}$$

In computing the fatigue life according to equation (8), it should be noted that the summation appearing in the denominator should be limited to the steady-state modes of the response, i.e. the values of i such that $\zeta_i\approx 0$, since the transient modes will generate only small damage. Further, the application of the above concepts to simplified structural models of the blades is not immediate as the detailed geometry of the blade has been lost and the corresponding stress distribution cannot be recovered exactly. It is, however, possible to compare the fatigue lives obtained under different flow conditions, wake models, etc., by considering the "equivalent stress",

$$\sigma_{\mathrm{eq}}(t)=\sqrt{\tfrac{1}{2}k_h h^2(t)+\tfrac{1}{2}k_\theta\theta^2(t)}\,\left[\sqrt{k_h/c^2+k_\theta/c^4}\right]. \tag{9}$$

Note that the above definition of the equivalent stress is not only dimensionally but also physically admissible since it is proportional to the square root of the energy of deformation in the system.

The absolute values of the fatigue life thus obtained will not be correct, but the ratio of two estimates obtained in connection with two different situations (having the same blade geometry and material properties) will be accurate. Since the objective here is to assess the effect of flow-induced vibrations on fatigue life, a relative comparison is sufficient.

2.5. Energy Transfer

The technique used for the estimation of fatigue life in the present investigation yields results that are directly comparable only when the structural properties of the blades are identical. Because of the simplifications involved by the two-degree-of-freedom structural model (3), many of the local material characteristics (including the stress distribution) are lost. In order to be able to compare resonance cases for which the structural properties are different, the concept of energy transfer between fluid and structural system is introduced instead. Thus, the structural dynamic equations (3a) for bending and (3b) for torsion are multiplied by $\dot{h}$ and $\dot{\theta}$, respectively. The resultant equations are integrated with respect to time over one period. Since only the harmonic oscillations are of interest, the integrals on the left-hand side of the respective equations vanish, and after adding the two resulting integrals, it follows that

$$q_D c \frac{\omega}{2\pi} \int_0^{2\pi/\omega} C_L \dot{h}\, \mathrm{d}t + q_D c^2 \frac{\omega}{2\pi} \int_0^{2\pi/\omega} C_M \dot{\theta}\, \mathrm{d}t = 0, \tag{10}$$

where q_D is the dynamic pressure and the period is $2\pi/\omega$. Equation (10) indicates that the total power, which is generated by the aerodynamic coefficients, should be zero. The aerodynamic coefficients can be decomposed into a damping part and an externally generated part, which from the energy point of view should balance each other.

Finally, the power input (energy transfer) from the fluid can be assessed by computing the damping associated with a certain harmonic oscillation. It is given by

$$P_{\text{in}} = -q_D c \frac{\omega}{2\pi} \int_0^{2\pi/\omega} (C_L)_{\text{damp}} \dot{h}\, \mathrm{d}t - q_D c^2 \frac{\omega}{2\pi} \int_0^{2\pi/\omega} (C_M)_{\text{damp}} \dot{\theta}\, \mathrm{d}t, \tag{11}$$

where $(C_L)_{\text{damp}}$ and $(C_M)_{\text{damp}}$ are the damping part of C_L and C_M, respectively. In order to compare the effect of the fluid resonance on the structural response of the system, equation (11) is used to assess the energy supplied by the fluid medium to the blade.

3. AERODYNAMIC/STRUCTURAL RESONANCE

3.1. Physical Modeling Aspects

Before embarking on the detailed analysis of the flow-induced vibration problem created by an oncoming flow with a KVS excitation pattern superimposed on the free-stream, it would be instructive to speculate on the possible physics of the problem. Since the EIE has a fundamental frequency of c/d, it is natural to expect that this would play an important role in the response of the blade. This is obvious from an examination of the limiting situations shown in Figure 2. Blade 1 extends over many wavelengths; therefore, the blade experiences a large number of chordwise fluctuations of the boundary conditions. These fluctuations cancel each other, thus yielding a limited response in terms of aerodynamic coefficients. In other words, the influence of the fluctuations is averaged off by integration. On the other hand, blade 2 extends over just one-half of the excitation wavelength ($c/d = 0{\cdot}5$); therefore, it experiences throughout its chord length the same type of perturbation, and there is no averaging effect. This, in turn, leads to a larger response than that represented by blade 1.

Many researchers have tackled similar problems in the past. Among them, Knoller (1909), Betz (1912) and Katzmayr (1922) have concentrated on increasing the efficiency of a harmonically oscillating airfoil in order to emulate the flight of birds. The basic assumption in these early studies is that the airfoil is influenced only by a monochromatic harmonic gust. Later, Schmidt (1960, 1965) re-examined the problem with the aim to improve the

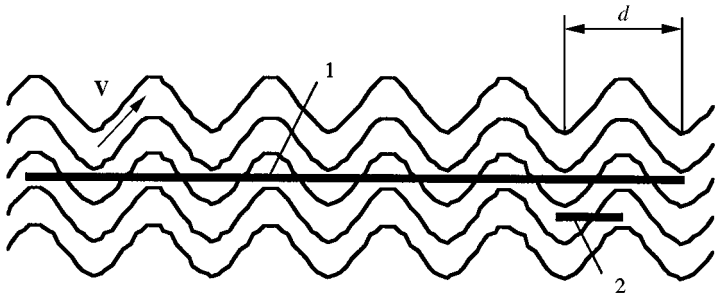

Figure 2. The effect of a harmonic excitation on two airfoils of different chord length.

thrust efficiency of oscillating airfoils in a tandem configuration. The downstream airfoil was positioned so as to convert into thrust part of the wake energy generated by the upstream airfoil. Schmidt observed that the highest propulsive efficiency is reached when the chord length of the receiving airfoil equals 75% of the wavelength of the oscillation.

Recently, the propulsive effectiveness and flow characteristics of an oscillating airfoil in the presence of a vortical flow has been examined experimentally (Gopalkrishnan *et al.* 1994) and numerically (Streitlien *et al.* 1996). The vortical flow was generated by an upstream cylinder in the experimental study and was specified to be a KVS in the numerical work. In these studies, the airfoil was excited externally and the imposed oscillations have a prescribed amplitude and frequency. A rigid airfoil was used because the studies were concentrated on the effects of the oncoming vortical flow on the propulsive effectiveness. They found that the propulsive effectiveness was governed by the phase between the motion of the airfoil and the arrival of the oncoming vortices. However, evidence in support of the present interpretation discussed above can be extracted from the experimental work of Gopalkrishnan *et al.* (1994). From their results, it can be inferred that the transfer of energy between the cylinder vortices and the airfoil is close to a maximum for the case where the chord length is $2d_u$ and the axial distance between cylinder vortices is $3{\cdot}5d_u$. Here, d_u is the diameter of the cylinder used to generate the oncoming vortices. Even though their case is slightly different from the present problem, nonetheless, their results lend credence to the interpretation made above.

These findings support the idea that the aerodynamic response of a blade subject to a KVS excitation is governed by a phenomenon, tentatively called "aerodynamic resonance" for lack of a more appropriate term, that leads to a sizable increase of the aerodynamic response when the chord of the blade equals about half of the wavelength of the excitation. Evidence in support of this interpretation is provided below. In order to demonstrate that the phenomenon is purely an aerodynamic behavior and not a structural manifestation, results on a rigid blade are presented first. This is followed by results on an elastic blade, where the aerodynamic resonance still plays an important role in the resulting fluid-structure interactions.

3.2. Computational Aspects

One of the objectives of this analysis is to show that the frequency parameter c/d has a strong influence on the level of the aerodynamic response to a KVS excitation pattern. All calculations were carried out with two release points for the vortices and they are located at $x = -1{\cdot}0$, $y = 0{\cdot}3$ and $x = -1{\cdot}0$, $y = -0{\cdot}2$ and a nondimensional strength of the vortices equal to $\Gamma = 0{\cdot}1$ (corresponding to a lift coefficient of $C_L = 0{\cdot}2$ for the given blade). Here,

TABLE 2

Coordinates of the T1 blade

N	X	Y	N	X	Y	N	X	Y
1	0·98744	0·15796	33	0·11890	0·07554	65	0·13041	0·16456
2	0·98449	0·15626	34	0·09690	0·06488	66	0·15411	0·17884
3	0·98256	0·15669	35	0·07740	0·05435	67	0·17744	0·19167
4	0·97142	0·16103	36	0·06182	0·04485	68	0·20448	0·20528
5	0·95581	0·16869	37	0·04726	0·03479	69	0·23291	0·21834
6	0·93624	0·17842	38	0·03493	0·02537	70	0·26241	0·23071
7	0·91365	0·18895	39	0·02218	0·01498	71	0·29264	0·24220
8	0·86491	0·20685	40	0·01370	0·00818	72	0·32330	0·25264
9	0·83802	0·21304	41	0·00641	0·00308	73	0·35407	0·26189
10	0·81044	0·21697	42	0·00000	0·00000	74	0·38217	0·26919
11	0·78226	0·21899	43	− 0·00161	0·00138	75	0·41277	0·27580
12	0·75351	0·21944	44	− 0·00399	0·00470	76	0·44360	0·28099
13	0·72426	0·21865	45	− 0·00555	0·01372	77	0·47489	0·28474
14	0·69457	0·21695	46	− 0·00483	0·01923	78	0·50700	0·28706
15	0·66702	0·21488	47	− 0·00321	0·02532	79	0·54010	0·28790
16	0·63657	0·21217	48	− 0·00072	0·03193	80	0·57161	0·28737
17	0·60564	0·20892	49	0·00081	0·03539	81	0·60735	0·28536
18	0·57411	0·20499	50	0·00255	0·03895	82	0·63496	0·28282
19	0·54189	0·20029	51	0·00438	0·04261	83	0·68212	0·27660
20	0·50891	0·19472	52	0·00657	0·04633	84	0·72044	0·26975
21	0·47503	0·18817	53	0·00884	0·05013	85	0·75892	0·26116
22	0·44317	0·18122	54	0·01121	0·05399	86	0·79722	0·25078
23	0·40772	0·17268	55	0·01385	0·05791	87	0·83186	0·23963
24	0·39879	0·17042	56	0·01658	0·06186	88	0·86849	0·22593
25	0·36304	0·16087	57	0·01945	0·06584	89	0·90263	0·21132
26	0·32753	0·15071	58	0·02245	0·06986	90	0·93287	0·19664
27	0·29266	0·14010	59	0·02558	0·07388	91	0·95783	0·18265
28	0·25885	0·12921	60	0·03802	0·08862	92	0·97611	0·17020
29	0·22918	0·11913	61	0·05316	0·10442	93	0·98631	0·16005
30	0·19853	0·10814	62	0·06993	0·11991	94	0·98744	0·15796
31	0·16985	0·09719	63	0·08836	0·13395			
32	0·14323	0·08632	64	0·10852	0·14999			

x is the stream direction and y is the transverse direction. In order to demonstrate that the phenomenon is not influenced by the geometry of the blade, calculations were carried out using two entirely different blades. They are a symmetrical 12% thick NACA 0012 airfoil section (Abbott and von Doenhoff 1959) and a high loading turbine blade (T1) that is typical of turbomachinery applications. The two blades used have identical chord length, c. Details of the T1 blade geometry are given in Table 2. In this table, X and Y are the nondimensional coordinates, normalized with respect to c. Rigid blades are considered first in order to investigate the influence of c/d on the aerodynamic response in the absence of structural interactions. The parameter c/d was varied in the range, 0·1–5·0. The number of time-steps used in the computations is 10000 with $\delta t = 0{\cdot}05$. This period is sufficiently large to avoid the effects of initial conditions; in other words, stationarity in all calculated time histories has been fully established. In the present investigations, all calculations were carried out with $U_\infty = 100$ m/s (which is below flutter speed) and $c = 0{\cdot}2$ m. These were used as characteristic velocity and length scales.

The locations of the vortex release points are selected based on the following reasoning. It should be noted that the NACA 0012 airfoil and the T1 blade have completely different

aerodynamic loadings. Therefore, if a symmetric release is chosen based on the NACA 0012 airfoil, the T1 blade could find itself lying partially or completely outside of the KVS vortex pattern. Consequently, the one-half chord vertical separation (between $y = 0{\cdot}3$ and $y = -0{\cdot}2$) was chosen to ensure that this situation would not occur. It should be pointed out that the actual separation distance chosen is also affected by the value of $\Gamma(= 0{\cdot}1)$ adopted in the present study. A different Γ and a different aerodynamic loading would give rise to different release points in the y direction.

3.3. Effect of the Number of Panels

Before embarking on the study of aerodynamic resonance, an investigation was first carried out to examine the effect of the number of panels on the calculated results. Two separate calculations were performed on an elastic NACA 0012 airfoil using 35 and 185 panels each. The airfoil has structural properties as specified under E3 in Table 3. Of course, the natural frequencies for the NACA 0012 airfoil are different from those specified for the T1 blade in Table 3. A KVS pattern is prescribed in the upstream flow and the vortices are released at the locations $x = -1{\cdot}0$, $y = 0{\cdot}3$ and $x = -1{\cdot}0$, $y = -0{\cdot}2$. The calculated C_L time histories are shown in Figure 3(a). It can be seen that, within the accuracy of the numerical calculations, the difference between the two time histories is insignificant. This implies that the calculated statistics and spectrum will be essentially the same. On the other hand, there is a noticeable discrepancy in the calculated mean drag, $(C_D)_{\text{mean}}$, in the frequency range around $c/d = 0{\cdot}5$ [see Figure 3(b)]. The discrepancy is expected because the mean drag is very small and is not much larger than the estimated numerical error. It is comforting to know that $(C_D)_{\text{mean}}$ is essentially identical at frequencies outside of this frequency range. Even then, the trend displayed by both calculations is the same, namely that there is an increase in $(C_D)_{\text{mean}}$ around $c/d = 0{\cdot}5$, in spite of the fact that the magnitude of the increase is different. In view of this, it can be concluded that 35 panels are sufficient to give the correct C_L and the right trend for the calculated $(C_D)_{\text{mean}}$ behavior. Therefore, from this point on, all calculations were carried out using 35 panels.

3.4. Effect of Airfoil/Blade Geometry

This is demonstrated by considering rigid blades, so that there are no structural interaction effects present. However, before proceeding to actually show that aerodynamic resonance

Table 3

Structural characteristics of four different T1 blades

Parameter	E1	E2	E3	E4
c—blade chord (m)	0·2	0·2	0·2	0·2
m—blade mass (kg/m)	1·35	0·7	0·445	0·094
k_h—blade stiffness (plunging), (N/m^2)	3×10^5	$5{\cdot}5 \times 10^5$	$1{\cdot}1 \times 10^6$	$2{\cdot}595 \times 10^6$
I—blade moment of inertia (kg m)	$7{\cdot}8 \times 10^{-4}$	$7{\cdot}8 \times 10^{-4}$	$7{\cdot}8 \times 10^{-4}$	$7{\cdot}8 \times 10^{-4}$
k_θ—blade stiffness (pitching), (N)	9×10^4	9×10^4	9×10^4	$1{\cdot}046 \times 10^5$
a—elastic axis (% of chord)	45%	45%	45%	45%
x—center of gravity (% of chord)	37·5%	37·5%	37·5%	37·5%
f_h—bending natural frequency (Hz)	75	141	250	833
f_θ—pitching natural frequency (Hz)	2,189	1,915	1,833	1,875
$\hat{f}_h$—nondimensional f_h	0·15	0·282	0·5	1·666
$\hat{f}_\theta$—nondimensional f_θ	4·37	3·83	3·67	3·75

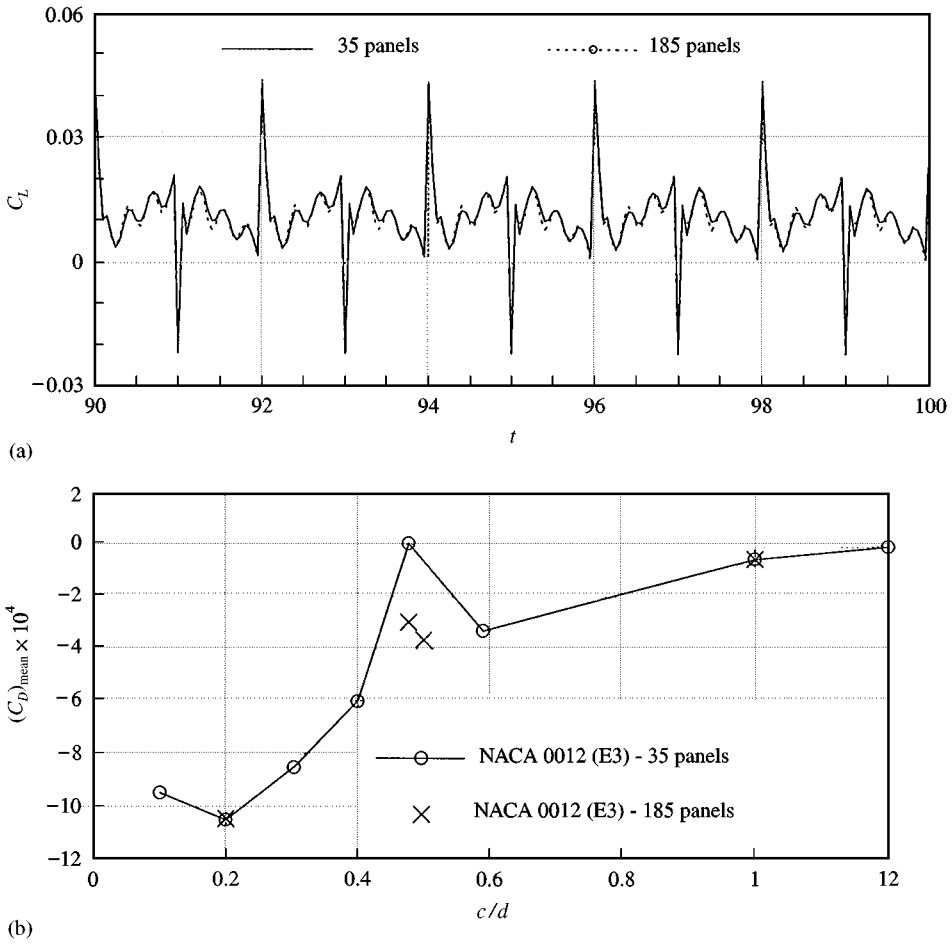

Figure 3. (a) Comparison of the calculated lift coefficient time histories; NACA 0012 airfoil with E3 structural properties (Table 3). (b) Comparison of the calculated mean drag coefficient; NACA 0012 airfoil with E3 structural properties.

exists under the action of an EIE, it is necessary to first examine the effect of geometry on the aerodynamic response. Results presented below correspond to several values of c/d. The first case is shown in Figure 4 with $c/d = 0{\cdot}1$. The wake structure at a nondimensional time $t = 500$ is shown together with the C_L time history over a period of ten cycles. This time period is chosen because it is representative of the EIE modes after the transient modes have been damped off. The same results for the T1 blade are shown in Figure 5. These two time-series (Figures 4 and 5) display similar features, except for the mean value of the response which is $(C_L)_{\text{mean}} = 0$ for the NACA 0012 airfoil and $(C_L)_{\text{mean}} = 1{\cdot}18$ for the T1 blade.

A second case with $c/d = 0{\cdot}5$ is presented in Figures 6 and 7. Again, the vortex structure at $t = 500$ and the C_L time history for a period of ten cycles are presented for the NACA 0012 airfoil and the T1 blade. Comparing the two time-series in Figures 6 and 7, it can be concluded again that the aerodynamic response is not as much affected by the geometry of the blade. Further, note that these C_L time histories closely resemble single

harmonic functions of frequency $d/c = 2{\cdot}0$ and are contrary to the results presented in Figures 4 and 5.

Finally, the vortex structure at $t = 500$ and the C_L time history over a ten cycle period for the NACA 0012 airfoil and the T1 blade at $c/d = 2{\cdot}0$ are shown in Figures 8 and 9, respectively. In this case, the density of the KVS vortex pattern has increased substantially as the number of vortices of the same strength released per unit time is much larger compared to the first two cases. However, the amplitude of the lift response is quite a bit smaller (Figures 8 and 9). This further substantiates the speculation that the aerodynamic response is significantly affected by the c/d ratio.

It should be pointed out that, within a given period, a positive and a negative vortex pass over the airfoil. The longitudinal positions of these vortices are not the same at the moment when a maximum or a minimum of the C_L response occurs. For example, in the case $c/d = 0{\cdot}5$, the C_L of the NACA 0012 airfoil has a maximum when the oncoming positive vortex is located at 89% chord and the negative vortex is located at 85% chord. For the T1 blade, the corresponding locations are 107 and 75%, respectively. Since the time step used in the calculations is 0·05, the resolution is no better than 5% chord in these determinations.

3.5. Aerodynamic Resonance

In order to show that the aerodynamic response indeed reaches a maximum at $c/d = 0{\cdot}5$, the $(C_L)_{\text{mean}}$ and $(C_M)_{\text{mean}}$ of the first harmonic and the root mean square (rms) values, $(C_L)_{\text{rms}}$ and $(C_M)_{\text{rms}}$, of C_L and C_M are calculated for a range of c/d and their distributions are plotted in Figures 10 and 11, respectively. Two strong peaks located around $c/d = 0{\cdot}5$ and 1·5 can be observed in the distributions of C_L, C_M, $(C_L)_{\text{rms}}$ and $(C_M)_{\text{rms}}$ for the NACA 0012 airfoil and the T1 blade. Besides the peaks located at $c/d = 0{\cdot}5$ and 1·5, one more peak is observed at $c/d = 2{\cdot}5$. Even though this general behavior is similar for both the NACA 0012 airfoil and the T1 blade, the values of the peaks differ for these two airfoils. In the $(C_L)_{\text{mean}}$ and $(C_M)_{\text{mean}}$ distributions of the NACA 0012 airfoil, the maximum value of the second peak ranges from about 60 to 80% of that of the first peak, while the maximum value of the third peak is at least several times smaller than that of the second peak. This is not quite the case for the T1 blade. In general, the second peak of the T1 blade is higher than the second peak of the NACA 0012 airfoil. Further, it is also noted that the second peak of the T1 blade is either higher or equal to its first peak. This quantitative behavior is different from that of the NACA 0012 airfoil. However, the third peak of the T1 blade is also substantially reduced compared to the first two peaks, similar to that observed for the NACA 0012 airfoil. One of the reasons for the quantitative difference in the peak values could be attributed to the high loading of the T1 blade. On the other hand, in the $(C_L)_{\text{rms}}$ and $(C_M)_{\text{rms}}$ distributions, the third peak is higher than the second peak. This is probably due to the interaction of the third harmonic of the KVS vortex pattern with the third harmonic of the aerodynamic response. The fact that this does not affect the first harmonic behavior suggests that the aerodynamic response is dominated by the first harmonic; an observation further supported by the spectral behavior shown in Figure 12. These results, therefore, indicate that the aerodynamic response of the airfoil/blade to the oncoming vortices is limited to about three chord lengths. In other words, over a frequency period of $0 < c/d < 3$, the aerodynamic response essentially decreases to close to zero. The major response is associated with $c/d = 0{\cdot}5$ though.

Since the distributions of the $(C_L)_{\text{mean}}$ and $(C_M)_{\text{mean}}$ of the first harmonic and the $(C_L)_{\text{rms}}$ and $(C_M)_{\text{rms}}$ for both the NACA 0012 airfoil and the T1 blade are essentially similar qualitatively, it can be concluded that the shape of the blade does not influence, at least trend-wise, the c/d dependence of the aerodynamic response. This implies that the higher

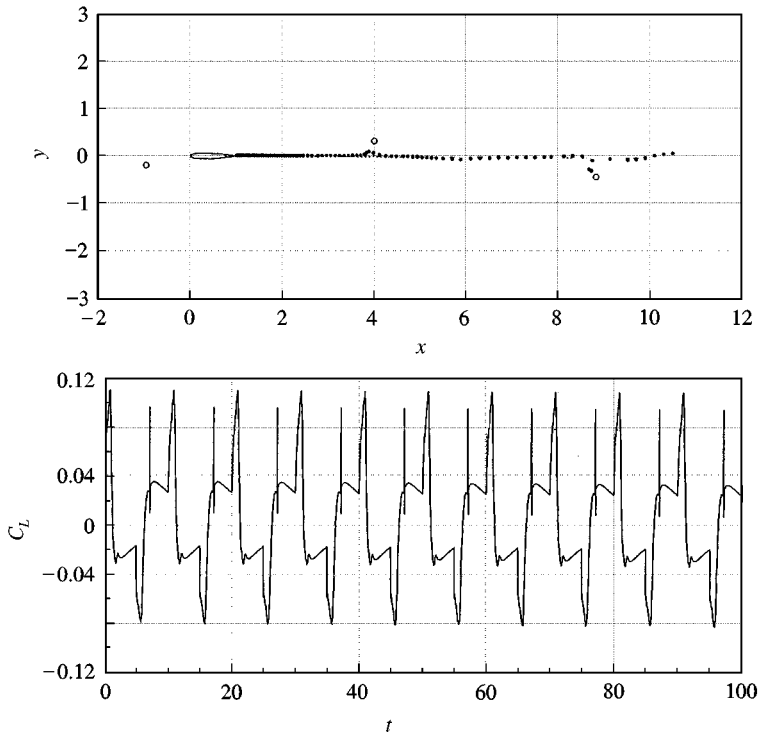

Figure 4. Rigid NACA 0012 airfoil with $c/d = 0{\cdot}1$; vortex structure and the instantaneous C_L time history.

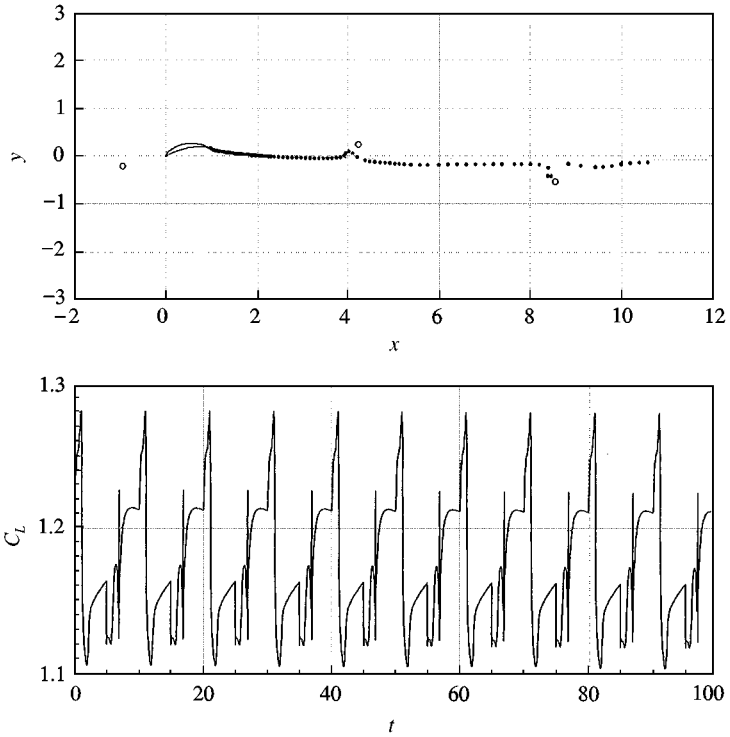

Figure 5. Rigid T1 blade with $c/d = 0{\cdot}1$; vortex structure and the instantaneous C_L time history.

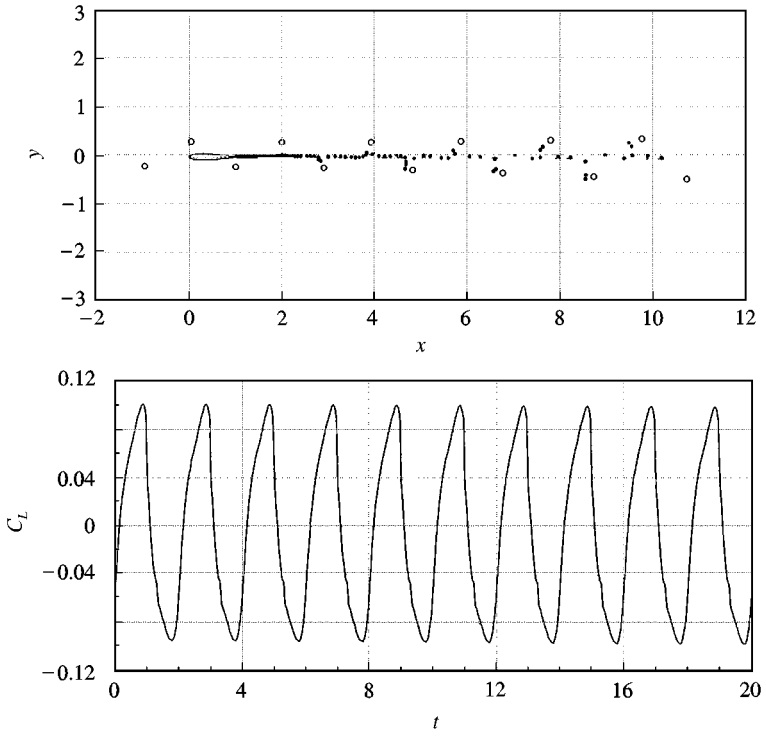

Figure 6. Rigid NACA 0012 airfoil with $c/d = 0{\cdot}5$; vortex structure and the instantaneous C_L time history.

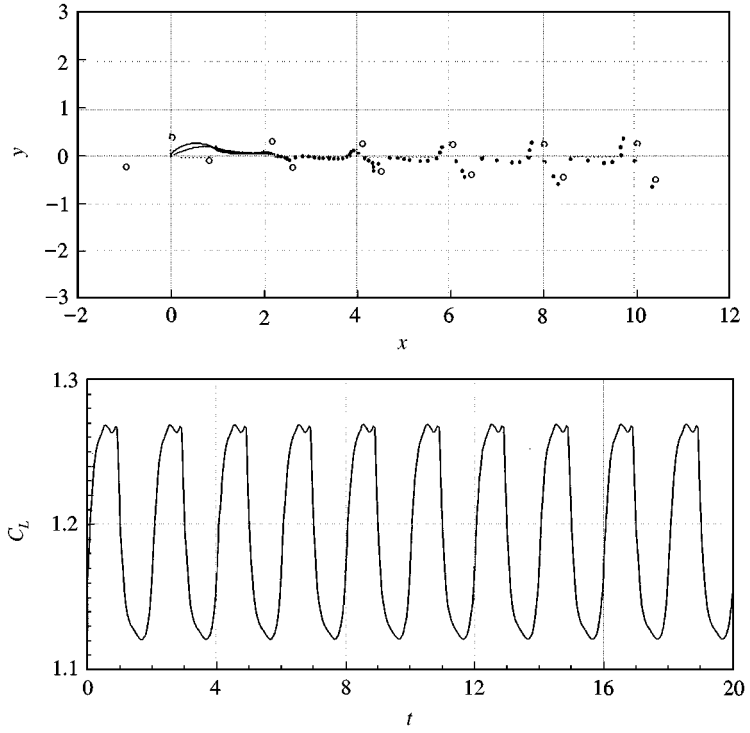

Figure 7. Rigid T1 blade with $c/d = 0{\cdot}5$; vortex structure and the instantaneous C_L time history.

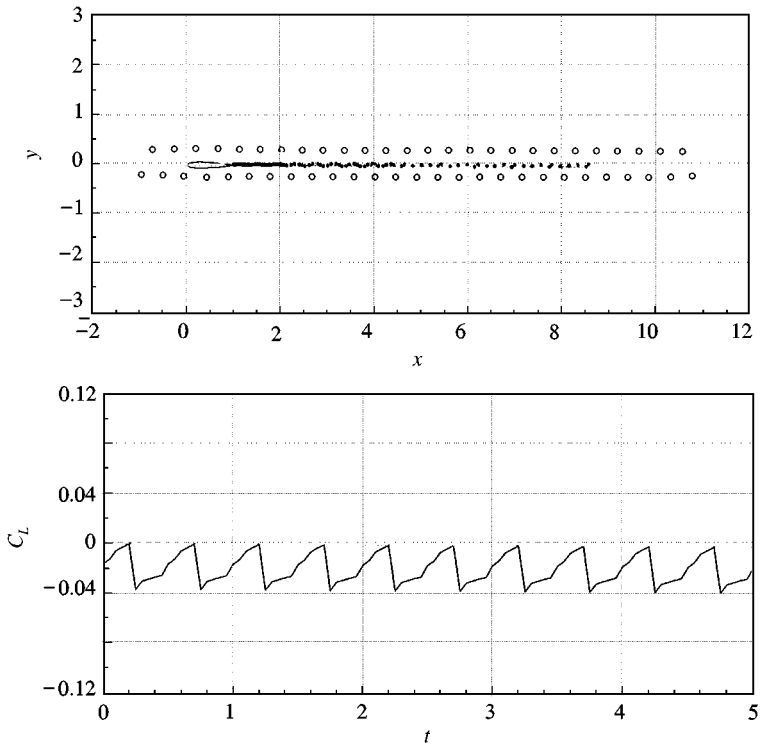

Figure 8. Rigid NACA 0012 airfoil with $c/d = 2{\cdot}0$; vortex structure and the instantaneous C_L time history.

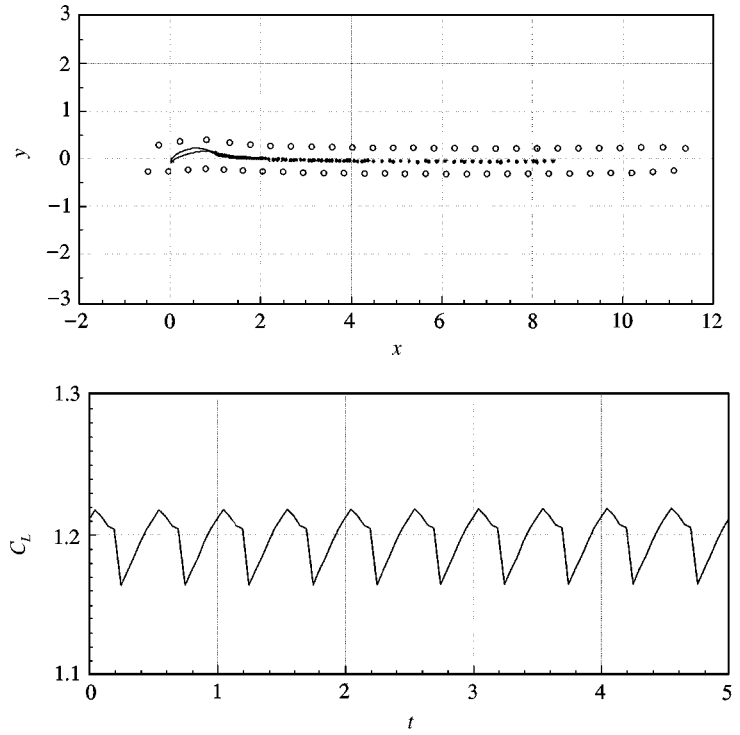

Figure 9. Rigid T1 blade with $c/d = 2{\cdot}0$; vortex structure and the instantaneous C_L time history.

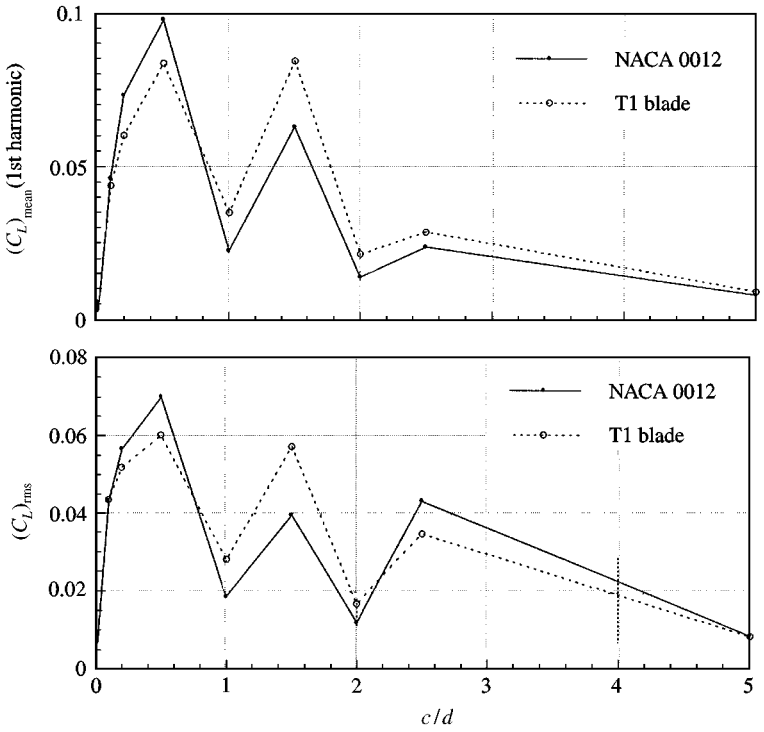

Figure 10. Variations of the mean amplitude of the first harmonic of C_L and $(C_L)_{\text{rms}}$ with c/d.

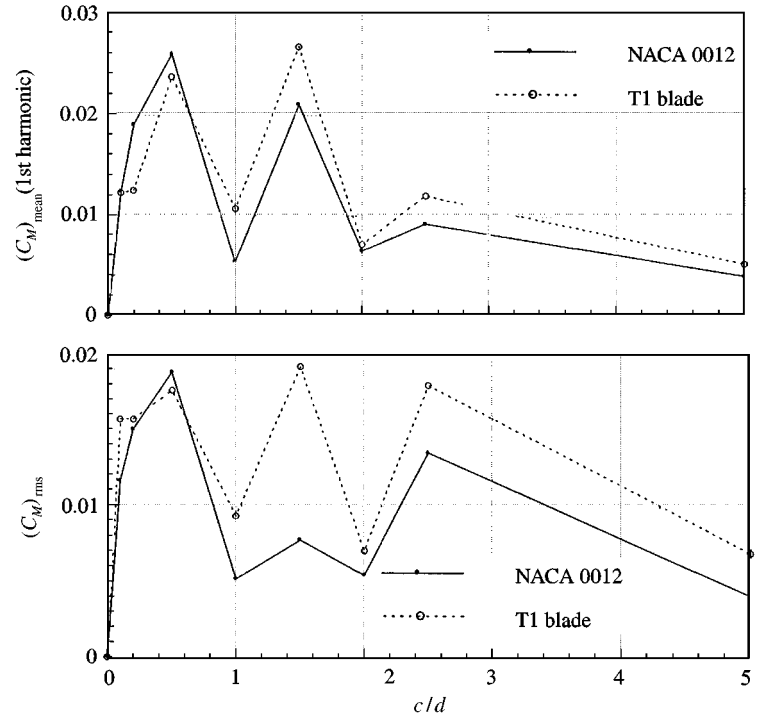

Figure 11. Variations of the mean amplitude of the first harmonic of C_M and $(C_M)_{\text{rms}}$ with c/d.

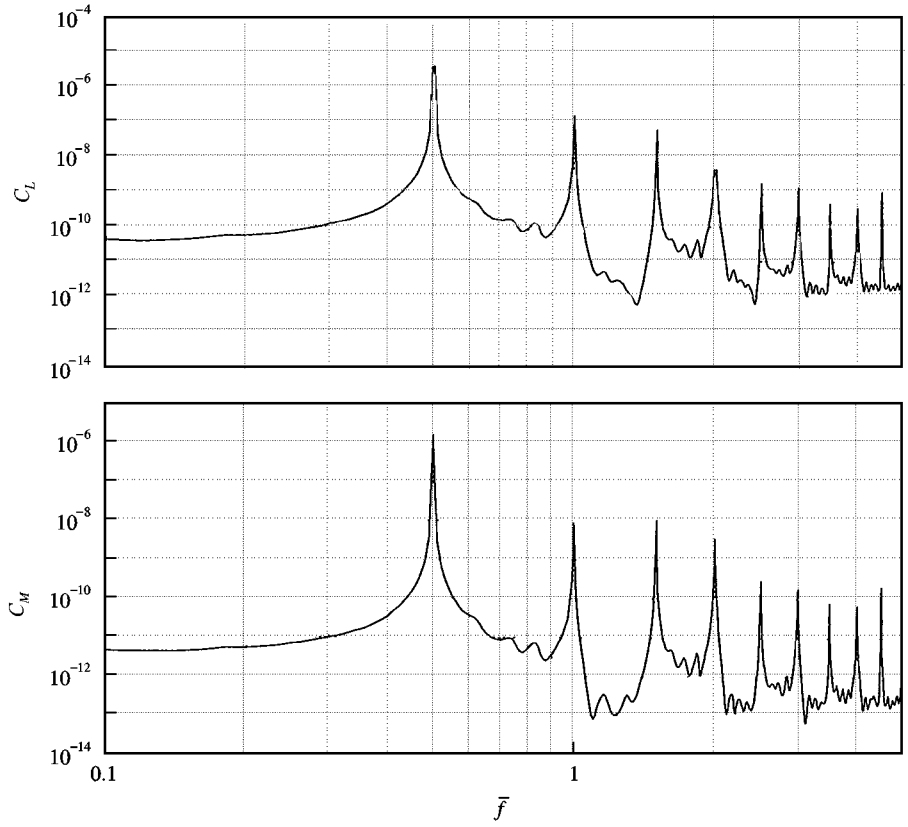

Figure 12. Power spectra for the C_L and C_M time histories of the rigid NACA 0012 airfoil; $c/d = 0{\cdot}5$.

harmonics, which are very easy to observe, for instance in Figure 4, do not alter the general characteristics of the aerodynamic response in general and the peaks located at $c/d = 0{\cdot}5$, $1{\cdot}5$ and $2{\cdot}5$ in particular. The observation that the basic trend of the phenomenon is guided by the first harmonic can be further inferred from Figure 12 which depicts the power spectra of the aerodynamic coefficients for $c/d = 0{\cdot}5$. These power spectra were determined using the same ARMA modeling technique as in Jadic *et al.* (1998); for details also see Mignolet and Red-Horse (1994). It can be observed that the peak corresponding to the first harmonic dominates all the others.

Together, these results show that there is indeed an aerodynamic resonance occurring at $c/d = 0{\cdot}5$ and $1{\cdot}5$ and that its occurrence is not a function of the blade geometry. In other words, the phenonmenon is not a consequence of fluid–structure interactions, rather it is purely an aerodynamic behavior.

3.6. Structural Resonance

The objective of this section is to assess the relationship between the resonance with the MIE modes, which is the classical structural resonance, and the aerodynamic resonance observed in the case of rigid blades; in other words, the fluid-structure interactions arise from the KVS vortex pattern. Since the aerodynamic resonance phenomenon is relatively indepenent of the blade geometry, from this point on, only the T1 blade with elastic

structural properties as listed under E4 in Table 1 was used in the calculations in this section. All the computations were carried out using the same KVS vortex pattern as that assumed for the rigid blades. The nondimensional frequency parameter c/d was varied from 0·1 to 3·35. A number of 10000 time steps with $\delta t = 0{\cdot}025$ was used for all the calculations. Again, this number of time-steps is sufficient to give results that are relatively independent of the initial conditions and show good convergency. Indeed, as an indication of the convergence of the computational process to a steady state solution, note that the damping ratios associated with the frequency c/d and all its harmonics were found to be very close to zero, i.e., less than 10^{-5}. The bending and pitching natural frequencies, f_n and f_θ, reported in Table 3 are the natural frequencies of the structure alone. It should be pointed out that the flow will modify these frequencies; therefore, the bending and pitching natural frequencies in a combined fluid-structure system will be different. These frequencies can be determined using ARMA to analyse the time series of h, θ, C_L or C_M of any one run with the elastic T1 blade. The bending and pitching natural frequencies of the combined fluid–structure system, f_n^* and f_θ^*, are determined to be 1·40 and 4·0, respectively.

The vortices of the KVS vortex pattern are released at $x = -1{\cdot}0$, $y = 0{\cdot}3$ and $x = -1{\cdot}0$, $y = -0{\cdot}2$ and they give rise to a steady state behavior. The main feature of such a behavior is characterised by an asymptotic approach of the response amplitude towards the steady state. The approach can involve either an increase or a decrease of the level of oscillations, depending on the position of the initial conditions with respect to the steady-state oscillations as can be seen from the phase plane plots. These plots for the nondimensional frequencies $c/d = 0{\cdot}2$, 0·69, 1·4 and 2·0 are shown in Figures 13–16.

Considering the $c/d = 1{\cdot}4$ case (Figure 15) first, it can be seen that the fundamental EIE frequency is close to the natural frequency of the lowest MIE mode which is primarily a bending mode. However, as a result of fluid–structure interactions, the lowest bending mode natural frequency is reduced to 1·4. Therefore, it is expected that a $c/d = 1{\cdot}4$ would lead to a resonance behavior with the lowest bending mode. When this occurs, the corresponding amplitude of the response would overwhelm the contributions of any other frequencies present. Consequently, a near perfect single harmonic behavior results. The circular character of the phase plot of h shown in Figure 15 is consistent with this speculation. An aerodynamic resonance is also observed at $c/d = 1{\cdot}5$, which is very close to

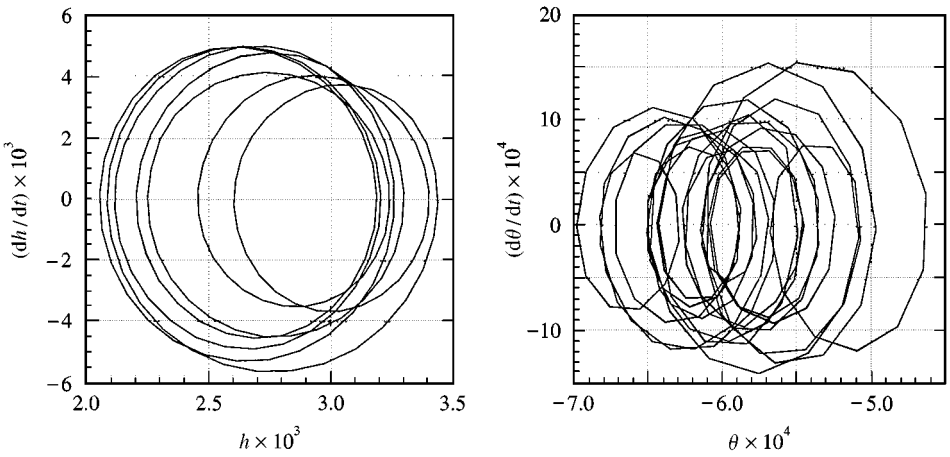

Figure 13. Phase plane plots for $c/d = 0{\cdot}2$; T1 blade with E4 properties.

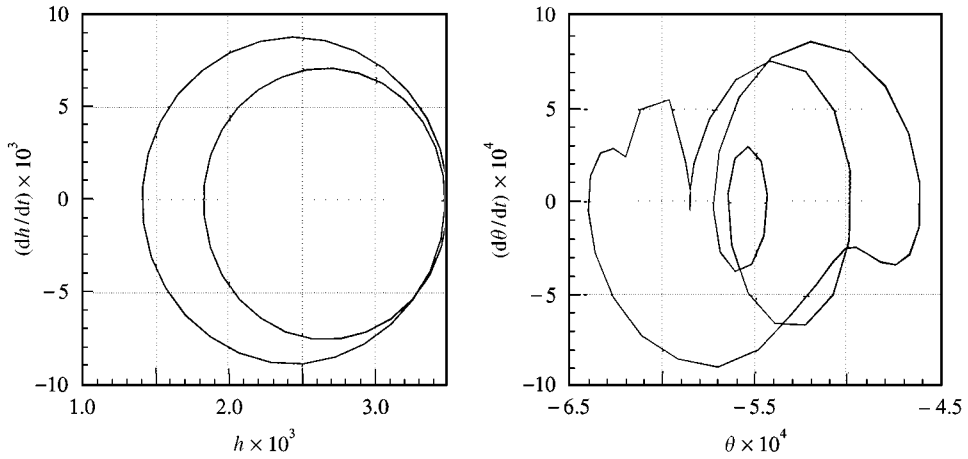

Figure 14. Phase plane plots for $c/d = 0{\cdot}69$; T1 blade with E4 properties.

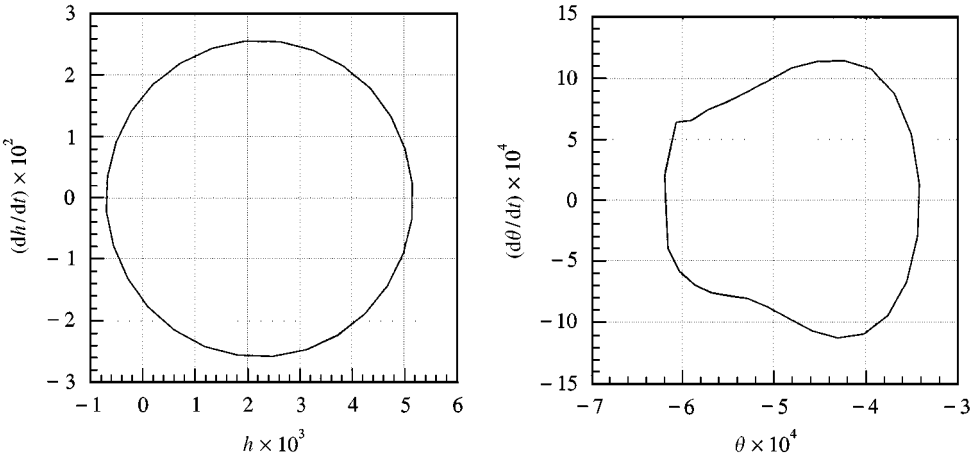

Figure 15. Phase plane plots for $c/d = 1{\cdot}4$; T1 blade with E4 properties.

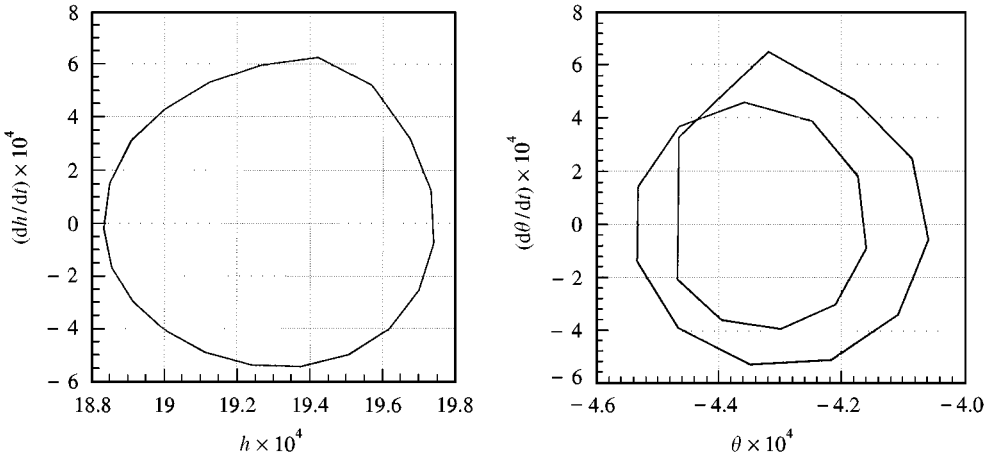

Figure 16. Phase plane plots for $c/d = 2{\cdot}0$; T1 blade with E4 properties.

1·4. However, its presence does not seem to affect the structural resonance behavior, except perhaps to modify the amplitude of the structural response. The calculations were carried out to $c/d = 3{\cdot}35$; however, the results do not show another peak at $c/d = 2{\cdot}5$. Consequently, the different distributions shown in Figures 17 and 18 are terminated at $c/d = 2{\cdot}0$.

Similar arguments can be put forward for the case of $c/d = 0{\cdot}69$. In this case, it is expected that the second harmonic of the bending response should prevail and hence the corresponding phase plane plot of h should consist of two nested loops. This is precisely what is shown

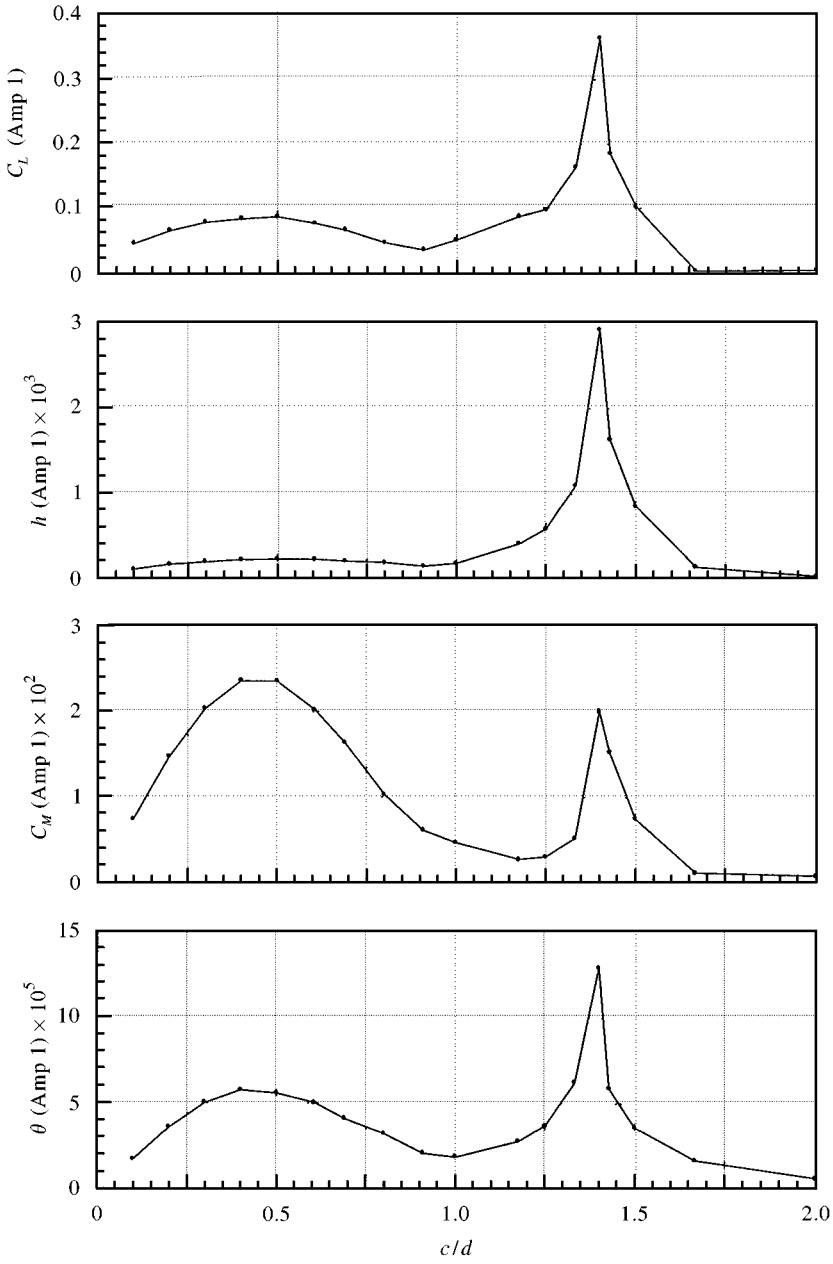

Figure 17. Variation of the first harmonic response with c/d for the T1 blade.

in Figure 14. If the frequency is further reduced to $c/d = 0{\cdot}2$, it could be expected that the bending response would primarily display a seventh harmonic of the EIE. This fact is confirmed by the seven nested loops of the phase plane plot of h shown in Figure 13. Finally, it should be noted that a similar situation occurs at $c/d = 2{\cdot}0$ (Figure 16) in connection with the torsional response, since the second harmonic of the EIE has a frequency that is close to the natural frequency of the MIE (mainly torsional) mode. This component is dominant in the torsional response and its corresponding phase plane plot displays two approximate nested loops (Figure 16).

Distributions of the amplitudes of the fundamental harmonics of the aerodynamic coefficients and the structural responses as a function of c/d are presented in Figure 17. All the responses in Figure 17 display a distinct peak corresponding to the structural resonance ($c/d = 1{\cdot}4$). Another peak, though flatter but clearly visible, has its maximum occurring at about $c/d = 0{\cdot}5$. This location corresponds to that where aerodynamic resonance occurs. The peak associated with the aerodynamic resonance at $c/d = 1{\cdot}5$ has been absorbed into the structural resonance at $c/d = 1{\cdot}4$ (Figure 17) for the reason given above. The calculations have been carried out to 3·5 and the results do not show another peak at $c/d = 2{\cdot}5$. These results, therefore, show that fluid–structure interactions tend to minimize the higher harmonic aerodynamic responses compared to the rigid airfoil/blade case shown in Figures 10 and 11. In view of these findings, it can be concluded that the aerodynamic resonance is not significantly affected by the presence of structural resonance.

Finally, the variations of the amplitudes of the second harmonics of the structural response with c/d are presented in Figure 18 together with their rms values. These results are very similar to those shown in Figure 17. They demonstrate that the methodology used for the present computations is capable of modeling higher harmonic interferences (Jadic *et al.* 1998), as evidence by the presence of peaks at locations corresponding to the second harmonic resonance between the EIE and the bending MIE modes.

4. DISCUSSION

Having examined the aerodynamic and structural resonance produced by oncoming vortices such as that given by a KVS pattern, the next step is to use the information thus obtained to assesss the relative damage on blade fatigue life, the energy transfer between the fluid and the structural system and the generation of thrust as a result of the interaction of the oncoming vortices with the wake vortex of the blade. The impact of the aerodynamic and structural resonance on these phenomena is discussed below separately. For the purpose of the present investigation, structural resonance is considered to happen when, for a given fluid–structure system, the EIE fundamental frequency equals the bending MIE frequency.

4.1. Impact on Blade Fatigue Life

Based on the above formulation, an estimate of the relative fatigue life of the T1 blade with E3 structural properties has been carried out. It should be emphasized that the present results have limited relevance in absolute values, but for the same geometry and structural properties they give a fairly accurate assessment of the impact of c/d on the blade fatigue life. The blade material properties have been assumed to be identical to those for "S96" steel (Harris 1961). Only the results for the relative damage D computed based on the first three harmonics are reported in Table 4. It is obvious from Table 1 why D is calculated based on the first three harmonics. Beyond that, the contribution of the higher harmonics to damage

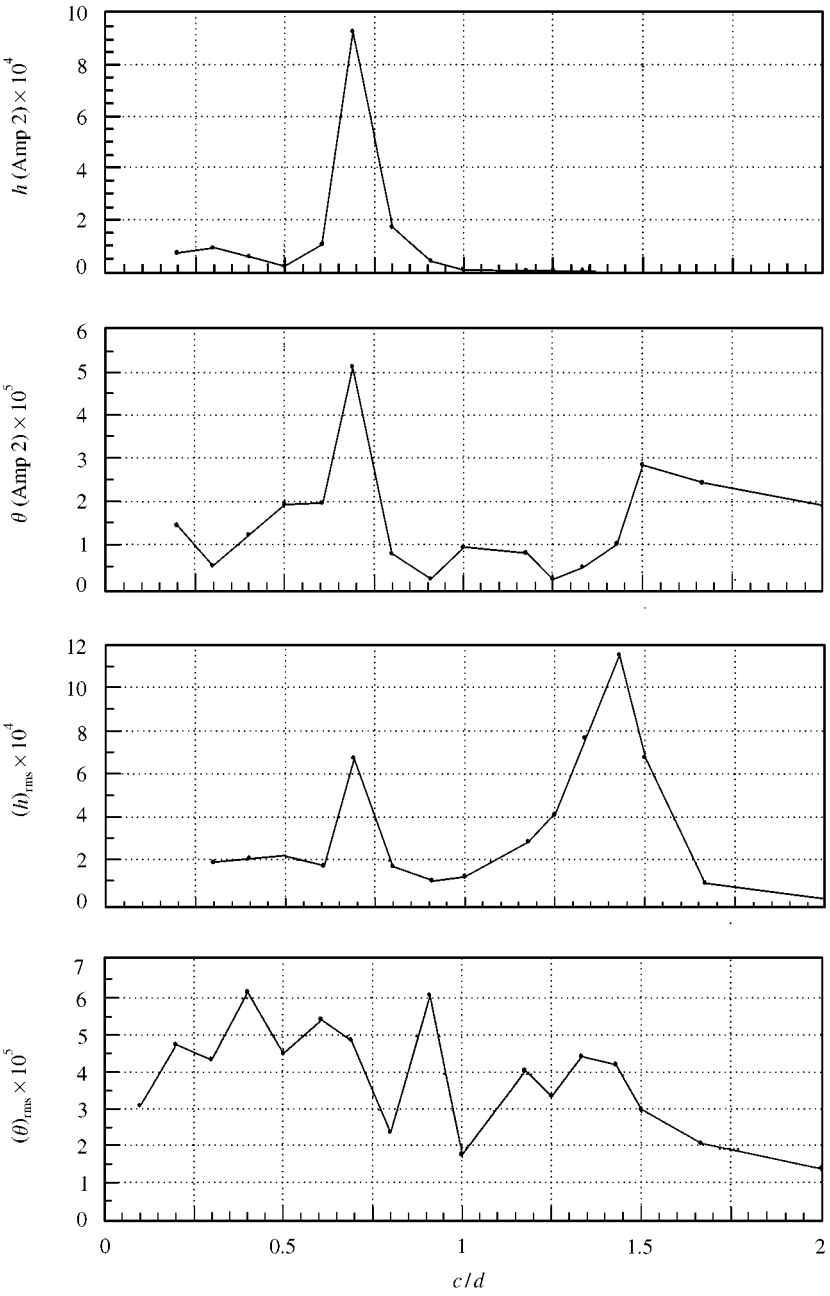

Figure 18. Variation of the second harmonic and rms response with c/d for the T1 blade.

estimate is relatively small. A total of 18 different c/d cases were calculated. In all the cases considered, the damage D was normalized by the result obtained at the aerodynamic resonance location, $c/d = 0{\cdot}5$. Therefore, a value greater than one means a lower blade fatigue life than that estimated for $c/d = 0{\cdot}5$.

TABLE 4

Relative damage D versus c/d for the elastic T1 blade with E3 properties

c/d	0·1	0·2	0·299	0·4	0·5	0·606	0·69	0·8	0·909
D	0·004	0·036	0·109	0·206	1·0	0·373	196·5	0·547	0·095
c/d	1·0	1·176	1·25	1·333	1·4	1·429	1·667	2·0	2·857
D	0·227	6·945	28·91	358·2	17191	1843	0·185	0·025	0·0001

The results show that the influence of structural resonance on fatigue life is overwhelming. Comparing the peaks due to structural resonance with the one at aerodynamic resonance, it can be observed that at the resonance of the second harmonic of c/d with f_n ($c/d = 0{\cdot}69$), the damage created is two orders of magnitude higher than at the aerodynamic resonance. At the resonance condition for the fundamental harmonic (i.e. $c/d = 1{\cdot}4$), the situation is even further amplified; the damage is four orders of magnitude greater than at the aerodynamic resonance conditions ($c/d = 0{\cdot}5$). Thus, the fatigue life is decreased by a factor of 10^2 and 10^4, respectively, in these two cases. Further, it should be pointed out that the peaks (due to structural resonance) are very narrow, for instance a 2% change in c/d from 1·429 to 1·4 changes the relative damage factor by one order of magnitude. This situation is clearly associated with the low damping ratio of the bending mode.

4.2. ENERGY TRANSFER

The effects of the aerodynamic resonance on a fluid–structure system already experiencing structural resonance ("double resonance condition") is discussed next. To this end, different fluid–structure systems were considered. They all have the same T1 blade geometry and the same KVS vortex pattern. However, they possess different structural properties; these are specified in E1 to E4 of Table 3. Also listed in the table are the normalized frequencies, $\bar{f}_h$ and $\bar{f}_\theta$, corresponding to the fundamental bending and torsional MIE mode for zero flow conditions, respectively.

The focus of this analysis was on the energy transfer between the fluid and the structure as described by equation (11). The different terms in this equation were evaluated as follows. First, the aerodynamic and structural responses were evaluated at resonance with the zero flow conditions, i.e., for $c/d = \bar{f}_h$, see Table 3. Then an ARMA analysis of the produced time series and an ensuing modal reconstruction similar to equation (2) yielded the amplitudes of each of the harmonics present in the response (for details see Jadic *et al.* 1998). Given these amplitudes, the power input from the vortex EIE to the oscillating system was evaluated according to equation (11). The aerodynamic damping required by equation (11) was computed by using Theodorsen's function (Fung 1993) with the amplitudes corresponding to the steady-state oscillations observed for each of the resonant structural systems.

The results of this study are presented in Table 5 with the input power P_{in} normalized by the value obtained in connection with the E3 structural system. It is obvious from this table that the power input to the system can be 20 times larger for systems with MIE natural frequencies coinciding with the aerodynamic resonance than for systems displaying a "simple" structural resonance. Therefore, "double" resonance (structural and aerodynamic) leads to an increased power input from the vortex EIE to the structure and thus can be the source of an additional increase in the damage produced and a corresponding decrease in the fatigue life of the blade.

TABLE 5

Relative power transfer versus non-dimensional frequency c/d for T1 blades with different structural characteristics at MIE resonance.

Structural characteristics	E1	E2	E3	E4
c/d	0·15	0·282	0·476	1·4
P_{in}	0·025	0·067	1·0	0·054

4.3. THRUST GENERATION

Schmidt (1960, 1965) analyzed the performance of a novel propulsive device consisting of a tandem blade configuration in which the leading blade is elastic, while the rear blade is rigid. The role of the latter is to improve the overall efficiency of the device by generating additional thrust from the energy provided by the vortex wake shed by the upstream moving blade. Schmidt observed that this device, labeled as the "wave propeller", achieves a maximum efficiency when the chord of the rear blade equals 75% of the wavelength of the leading blade oscillation. The propulsive efficiency η was defined (Garrick 1936) as

$$\eta = \frac{\bar{D}U_\infty}{\overline{W}}, \tag{12}$$

where $\bar{D} = (C_D)_{\text{meaan}}\,\rho U_\infty^2\, c/2$ is the mean drag and $\overline{W}$ is the mean power input required to move the forward blade. The mean drag coefficient is then given by

$$(C_D)_{\text{mean}} = \bar{f}\int_0^{u\bar{f}} C_D(t)\,\mathrm{d}t, \tag{13}$$

where $\bar{f} = fc/U_\infty$ is the nondimensional frequency.

In order to assess the effect of vortex excitation pattern on drag reduction, a configuration consisting of a NACA 0012 airfoil and a KVS pattern (Figure 1) is considered. The results for both the rigid airfoil and for the elastic airfoil with E3 properties are presented in Figure 19. It can be observed that for the rigid airfoil, the mean drag starts to decrease steeply around $c/d = 0{\cdot}5$, which is coincident with the location where aerodynamic resonance occurs. However, the maximum thrust is approximately $(C_D)_{\text{mean}} = -0{\cdot}001$ and occurs at around $c/d = 0{\cdot}2$. For the elastic airfoil with E3 properties, the trend is completely similar, except that at the point where resonance between the MIE and EIE modes occurs ($c/d = 0{\cdot}476$) there is a jump in the value of the mean drag to zero. For comparison, an estimate of the mean drag coefficient has been computed based on the data presented by Schmidt (1965). The overall agreement with the present calculations seems satisfactory, since in Schmidt's case the vortex excitation is not a KVS pattern, but rather it is a continuous vortex distribution that impinges on the blade.

The effect of blade geometry on the thrust generated by a KVS pattern is investigated next. Calculations were carried out for three different rigid blade shapes, which include the T1 blade and the NACA 0002 and NACA 0012 airfoils. The calculated $(C_D)_{\text{mean}}$ are compared in Figure 20. Both the thin and thick airfoils show a maximum thrust at a location around $c/d = 0{\cdot}2$. However, the T1 blade shows a maximum thrust at a smaller value of c/d. The present calculations fail to demonstrate clearly the location of the

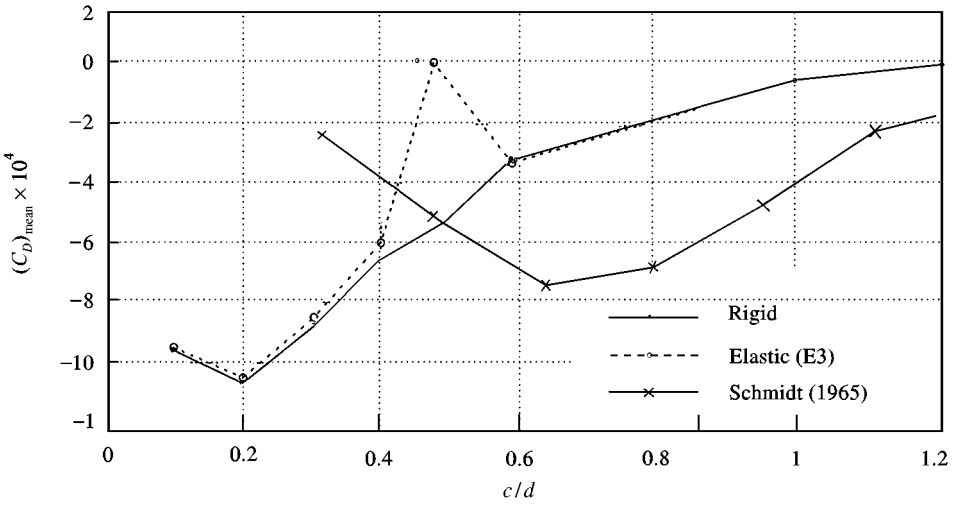

Figure 19. Variation of the mean drag coefficient of the NACA 0012 airfoil versus c/d.

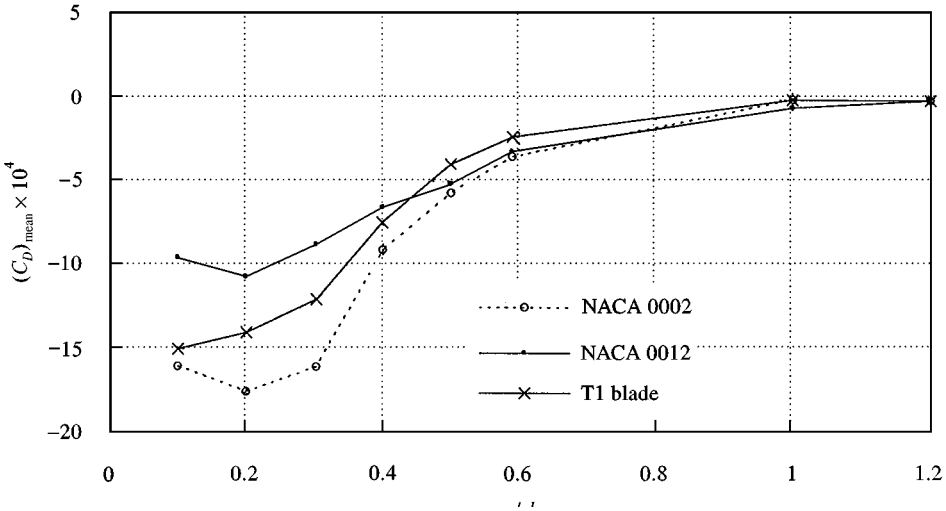

Figure 20. Comparison of the variation of the mean drag coefficient for three rigid airfoils.

maximum thrust, but they seem to support the interpretation that it occurs around $c/d = 0{\cdot}1$. Furthermore, the maximum thrust generated varies from blade to blade. It seems that the thrust generation is most effective for thin symmetrical airfoils with minimal loading, while the worst is for a thick symmetrical airfoil. In view of this, it can be said that the geometry of the blade and the wake it sheds interact with the oncoming vortex pattern in a very complicated way to produce the resulting thrust. There is no clear trend indicated here. Therefore, further investigation of this phenomenon is warranted.

5. CONCLUSIONS

The effects of oncoming vortices in a uniform flow on the aerodynamic and structural responses of an airfoil/blade have been investigated. They lead to a movement-induced

excitation (MIE), due to flow-induced vibrations arising from the uniform flow, and an extraneously induced excitation (EIE), due to the interactions of the oncoming vortices with the structural motion and/or its wake. Various vortex patterns have been considered for their relevance to turbomachinery applications. It is found that a Karman vortex street (KVS) is most representative of the shed vortices from a preceding blade row. Therefore, the KVS vortex pattern is adopted in the present investigation. A parameter related to the ratio of the chord length to the vortex spacing (c/d) is of fundamental importance and it is the effect of this parameter on the airfoil/blade response that is of interest in the present investigation.

The oncoming flow is assumed to be inviscid and the flow around the airfoil/blade remains attached to the surface. Aerodynamic effects due to the oncoming vortices are examined first by considering two different rigid airfoil/blade. One is a NACA 0012 airfoil while another is a turbine blade (T1) with very high aerodynamic loading. In this formulation, only the interactions of the oncoming vortices with the airfoil/blade wake vortices and their effects on the aerodynamic response are investigated. The results show that maximum responses are reached at $c/d = 0{\cdot}5$ and $1{\cdot}5$. Also, to a much lesser extent, another maximum is noted at $c/d = 2{\cdot}5$. This imples that the effect of the oncoming vortices on the airfoil/blade is limited to the frequency range, $0 < c/d < 3$. The response is similar qualitatively for the NACA 0012 airfoil and the T1 blade, thus suggesting that the behavior is not that depenent on the airfoil/blade geometry. This phenomenon is labeled "aerodynamic resonance". It should be emphasized that the present conclusion is valid only for an inviscid flow that remains attached to the airfoil/blade surface. In a viscous flow, geometry change could lead to separation and a totally different wake structure. Under these conditions, it is expected that the aerodynamic response would be quite different. Furthermore, the initial location of vortex release could also affect the aerodynamic response because the vortex strength will be influenced by viscous dissipation during the vortex approach to the airfoil/blade. The present finding corroborates well with the "undulating propeller" result of Schmidt (1965), which indicates that a maximum value of the propulsive efficiency of a tandem airfoil system can be achieved by choosing the receiving airfoil chord length to equal to $\sim 75\%$ of the wavelength of the oscillation of the leading airfoil.

The analysis of an elastic T1 blade shows the same "aerodynamic resonance" peak at $c/d = 0{\cdot}5$ in addition to other structural resonance peaks. However, the peak at $c/d = 1{\cdot}4$ is not observed. This is due to the fact that the structural properties of the T1 blade and the flow conditions chosen resulted in a bending MIE frequency of $c/d = 1{\cdot}4$. Consequently, the structural resonance merges with the aerodynamic resonance and gives rise to a single peak at $c/d = 1{\cdot}4$. Therefore, it can be concluded that the aerodynamic resonance is not significantly affected by the presence of structural resonance. Further, the power input from the fluid also displays a sharp maximum around the same value of $c/d = 0{\cdot}5$. These results are used to assess the relative damage to a turbine blade subject to this kind of flow-induced vibrations. For a T1 blade with E3 structural properties (Table 3), the blade fatigue life reduction produced by structural resonance is estimated to be four orders of magnitude compared to that given rise by the aerodynamic resonance. The aerodynamic resonance acting alone cannot bring a significant reduction of the blade fatigue life. However, the superposition of aerodynamic and structural resonance leads to dramatic increases of the power input (up to 20 times) from the vortex EIE (Table 5), which can be the source of an additional increase in the damage produced and a corresponding decrease in the fatigue life of the blade. Finally, the mean drag coefficient of a rigid NACA 0012 airfoil is found to become negative (i.e., thrust generation) around $c/d = 1{\cdot}0$; the same is also true for other airfoil/blade (Figure 20). The maximum thrust occurs at $c/d = 0{\cdot}2$ and the mean drag coefficient thus estimated is $(C_D)_{\text{mean}} = -0{\cdot}001$. The same calculations for a T1 elastic blade

with E3 structural properties show that aerodynamic and structural resonance acting together reduces thrust generation and, at $c/d = 0{\cdot}5$, $(C_D)_{\text{mean}}$ becomes zero again (Figure 19).

ACKNOWLEDGMENTS

R.M.C.So and M.P.Mignelet are grateful to the support given to them by the Research Grants Council of the HKSAR under Grant Nos. PolyU 5159/97E and PolyU 5128/98E and The Hong Kong Polytechnic University under Grant No. G-YW04. Part of this work was also carried out with support given to the first two authors (R.M.C.So and I. Jadic) by the Naval Surface Warfare Center, Caderock Division, Department of the Navy, Bethesda, MD 20084, USA. This latter contract was monitored by Dr W. Tang.

REFERENCES

Abbott, I. H. & Von Doenhoff, A. E. 1959 *Theory of Wing Sections*. New York: Dover.

Baban, F. & So, R. M. C. 1991 Recirculating flow behind and unsteady forces on finite-span circular cylinders in a cross-flow. *Journal of Fluids and Structures* **5,** 185–206.

Bélanger, F., Païdoussis, M. P. & de Langre, E. De 1995 Time-marching analysis of fluid-coupled systems with large added mass. *AIAA Journal* **33,** 752–757.

Betz, A. 1912 Ein Beitrag zur Erklarung des Segelflugels. *Zeitschrift für Flugtechnik und Motorluftshiffahrt* **3,** 269–272.

Casadei, F. & Halleux, J. P. 1995 An algorithm for permanent fluid–structure interaction in explicit transient dynamics. *Computer Methods in Applied Mechanics and Engineering* **128,** 231–289.

Chorin, A. J. 1973 Numerical study of a slightly viscous flow. *Journal of Fluid Mechanics* **57,** 785–798.

Christiansen, J. P. 1973 Numerical simulation of hydrodynamics by the method of point vortices. *Journal of Computational Physics* **13,** 363–379.

Clements, R. R. & Maull, D. J. 1975 The representation of sheets of vorticity by discrete vortices. *Progress in Aerospace Sciences* **16,** 129–146.

Dieter, G. E. 1986 *Mechanical Metallurgy*, 3rd edition. New York: McGraw-Hill.

Feiereisen, J. M., Montgomery, M. D. & Fleeter, S. 1994 Unsteady aerodynamic forcing functions: a comparison between linear theory and experiment. *ASME Journal of Turbomachinery* **116,** 676–685.

Funazaki, K. & Nishiyama, T. 1989 Measurements of simulated wake/rotor interaction phenomena in turbomachinery. *Unsteady Aerodynamics and Aeroelasticity of Turbomachines and Propellers, Proceedings of the* 5*th International Symposium on* September 18–21, 1989 (eds: Pan Tianmin, Lu Yingjie, Yan Wenxuan and Wu Xiaolu), 287–300.

Fung, Y. C. 1993 *An Introduction to the Theory of Aeroelasticity*. New York: Dover.

Garrick, J. E. 1936 Propulsion of a flapping and oscillating airfoil. NACA Report No. 567.

Gopalkrishnan, R., Triantafyllou, M. S., Triantafyllou, G. S. & Barrett, D. 1994 Active vorticity control in a shear flow using a flapping foil. *Journal of Fluid Mechanics* **274,** 1–21.

Hall, K. C. 1994 Eigenanalysis of unsteady flows about airfoils, cascades, and wings. *AIAA Journal* **32,** 2426–2432.

Harris, W.J. 1961 *Metallic Fatigue*. New York: Pergamon Press.

Hodson, H. P. & Dawes, W. N. 1996 On the interpretation of measured profile losses in unsteady wake-turbine blade interaction studies. ASME Paper 96-GT-494.

Jadic, I. 1997 Flow-induced vibrations of turbomachinery blades. PhD thesis, Mechanical and Aerospace Engineering Department, Arizona State University, Tempe, AZ 85287, USA.

Jadic, I., So, R. M. C. & Mignolet, M. P. 1998 Analysis of fluid–structure interactions using a time marching technique. *Journal of Fluids and Structures* **12,** 631–654.

Katzmayr, R. 1922 Effect of periodic changes of angle of attack on behaviour of airfoils. NACA TM-147.

Kemp, N. H. & Sears, W. R. 1955 The unsteady forces due to viscous wakes in turbomachines. *Journal of the Aeronautical Sciences* **22,** 1–7; also 478–483.

Knoller, R. 1909 Die Gesetze des Luftwiderstandes. *Flug und Motortechnik* (*Wien*) **3,** No. 21, 1–7; also No. 22, 1–6.

Knoller, R. 1913 Zur Theorie des Segelflugels. *Zeitschrift für Flugtechnik und Motorluftshiffahrt* **4,** 13–14.

Lalanne, M., Berthier, P. & Der Hagopian, J. 1983 *Mechanical Vibrations for Engineers*. New York: John Wiley & Sons.

Majjigi, R. K. & Gliebe, P. R. 1984 Development of a rotor wake/vortex model; Vol. I – Final Report. NASA-CR-174849.

Mignolet, M. P. & Red-Horse, J. R. 1994 ARMAX identification of vibrating structures: model and model order determination. *Proceedings of the 35th Structures, Structural Dynamics, and Materials Conference*, Hilton Head, SC, April 18–20, pp. 1628–1637.

Naudasche, E. & Rockwell, D. 1994 *Flow-Induced Vibrations — An Engineering Guide*. Brookfield, VT: A.A. Balkema.

Olson, L. G. & Bathe, K. J. 1985 Analysis of fluid–structure interactions — a direct symmetric coupled formulation based on fluid velocity potential. *Computers & Structures* **21,** 21–32.

Poling, D. R., Dadone, L. & Telionis, D. P. 1989 Blade–vortex interaction. *AIAA Journal* **27,** 694–699.

Schmidt, W. 1960 Über die Abstimmung eines Schlagruderflugels mit Nachflugel. *Deutsche Flugtechnik* **4,** 350–352.

Schmidt, W. 1965 Der Wellpropeller, ein neuer Antrieb fur Wasser-. Land- und Luftfahrzeuge. *Zeitschrift für Flugwissenschaften* **13,** 472–479.

So, R. M. C. & Savkar, S. D. 1981 Buffeting forces on rigid circular cylinders in cross flows. *Journal of Fluid Mechanics* **105,** 397–425.

Streitlien, K., Triantafyllou, G. S. & Triantafyllou, M. S. 1996 Efficient foil propulsion through vortex control. *AIAA Journal* **34,** 2315–2319.

Xing, J. T. & Price, W. G. 1991 A mixed finite element method for the dynamic analysis of coupled fluid-solid interaction problems. *Proceedings of the Royal Society* A **433,** 235–255.

Yao, Z. X. 1993 Unsteady aerodynamics of blade-blade interactions. Ph.D. thesis, Mechanical and Aerospace Engineering Department, Arizona State University, Tempe, AZ 85287, U.S.A.

Yao, Z. X., Garcia-Fogeda, P., Liu, D. D. & Shen, G. 1989 Vortex/wake flow studies for airfoils in unsteady motions. AIAA Paper No. AIAA 89–2225.

Yao, Z. X., Jadic, I., So, R. M. C., Liu, D. D. & Tang, W. 1995 Flow-induced vibrations on a turbine blade in a blade row using a vortex dynamics model. *International Forum on Aeroelasticity and Structural Dynamics*, Manchester, U.K., 26–27 June, 1995.

Zienkiewicz, O. C. & Bettess, B. 1978 Fluid-structure dynamic interaction and wave forces — an introduction to numerical treatment. *International Journal of Numerical Methods in Engineering* **13,** 1–16.